ELSEVIER

Comput. Methods Appl. Mech. Engrg. 154 (1998) 229–264

Computer methods in applied mechanics and engineering

A two-step, two-field hybrid method for the static and dynamic analysis of substructure problems with conforming and non-conforming interfaces

Daniel Rixen[a,1], Charbel Farhat[b,*], Michel Géradin[a]

[a]*Laboratoire des Techniques Aéronautiques et Spatiales, Université de Liège, Rue Ernest Solvay, 21, B-4000 Liège, Belgium*
[b]*Department of Aerospace Engineering Sciences and Center for Aerospace Structures, University of Colorado at Boulder, Boulder, CO 80309-0429, USA*

Received 2 July 1995; revised 20 July 1996

Abstract

The need for assembling independent finite element substructure solutions arises in several engineering and scientific problems including the design and analysis of complex structural systems, component mode synthesis, global/local analysis, adaptive refinement, and parallel processing. In this paper, we discuss the solution of such problems by a two-field hybrid method where the substructures are jointed with low-order polynomial or piece-wise polynomial Lagrange multipliers, and present a Rayleigh–Ritz based smoothing procedure for improving the accuracy of the computed coupled solution in the presence of various substructure heterogeneities. We consider both conforming and nonconforming substructure meshes, and demonstrate the benefits of the proposed two-step solution method with several examples from structural mechanics. © 1998 Elsevier Science S.A.

1. Introduction

Many complex structural systems are constructed by assembling a set of substructures that are designed by different teams of engineers. The global behavior of such structures is often predicted by 'gluing' together the individual substructure analyses. In such cases, the submeshes associated with the substructures usually have non-conforming discrete interfaces (Fig. 1), mainly because: (a) the corresponding substructures can have different resolution requirements, (b) the submeshes are often designed by different analysts, and (c) these submeshes may be constructed using incompatible finite element models. Therefore, the global static and dynamic analyses of such structural systems often require the development of special finite element assembly and solution procedures [1–4].

The need for gluing together independent finite element solutions computed over incompatible submeshes also arises in several other applications including global/local analysis [5,6], flexible multibody dynamics [7], adaptive refinement [8], and parallel processing via substructuring [9–11]. The most popular approach for devising such a glue is to introduce Lagrange multipliers for enforcing an approximate geometric compatibility between the given substructures. In general, this results in a two-field hybrid method that relies on a well-understood saddle-point variational principle [12–17]. Other approaches such as collocation and discrete

[1] This work was done while this author was visiting the University of Colorado at Boulder.

* Corresponding author.

PII S0045-7825(97)00128-X

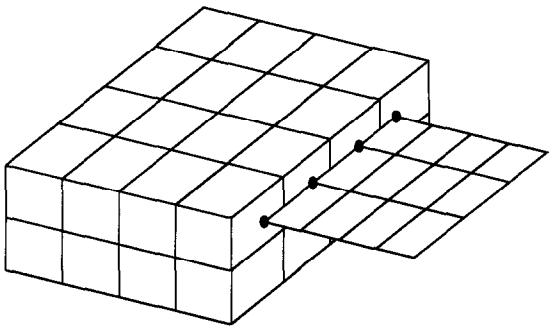

Fig. 1. Substructures with non-conforming interfaces.

least-squares formulations have also been investigated for assembling independent substructure analyses and found to be inferior to the Lagrange multiplier approach [8].

Two-field hybrid methods using an irreducible displacement formulation inside the substructures, and independently defined Lagrange multipliers on the substructure interfaces to join them are interesting not only for domain *integration*, but also for domain *decomposition* [13–16,18–20]. They provide a paradigm for constructing fast semi-iterative solvers that are attractive for parallel processing [11]. These solution methods are interesting even as serial algorithms, when the advantages that arise from isolating and solving the subproblems can be made to outweigh the additional work that is required for assembling the local solutions. In that case, the substructures are artificially generated by a mesh partitioning algorithm [21] and have compatible interfaces, which implies that discrete Lagrange multipliers can be used. However, when suitable low-order polynomial or piece-wise polynomial Lagrange multipliers are employed rather than discrete ones, a two-field hybrid method formulated for domain decomposition provides a mechanism for designing a useful model reduction algorithm [13–16]. Such an approach allows, for example, designing fast algebraic solvers that can exploit an eventual regularity of the solution at some spatial location [13–16], and simplifying the mesh generation tasks by making it computationally feasible to use the same mesh for both static and modal dynamic analyses [3,4,22].

For the above reasons, two-field hybrid methods have been recently gaining momentum for substructure applications with both matching and non-matching interfaces. Research so far has emphasized the proper approximation of the Lagrange multipliers—especially the satisfaction of the so-called Babuška–Brezzi or inf–sup condition [23,17]—and the fast algebraic solution of the resulting dual interface problem. Similar developments can also be found in the computational fluid dynamics literature, especially those articles related to the *mortar* method [24]. In this paper, we focus on different issues that have been motivated by our practical experience in using two-field hybrid methods with polynomial Lagrange multipliers for solving large and complex structural mechanics problems. These issues include the treatment of crosspoints for non-conforming substructures, the effect of various substructure heterogeneities on the accuracy of the coupled solution, and the elimination of parasitic eigenmodes when low-order polynomial Lagrange multipliers are employed. We present a new two-step, two-field hybrid method based on a Rayleigh–Ritz optimal smoothing procedure, and show that this discretization and solution method successfully addresses all the substructure issues raised above. For this purpose, the remainder of this paper is organized as follows.

In Section 2, we overview the basic two-field method for assembling independent finite element substructure solutions, and expose its deficiencies related to substructure heterogeneities and parasitic eigenmodes. In Section 3, we consider the case of a two-substructure problem with conforming interfaces and present a novel Rayleigh–Ritz based smoothing procedure for handling the difficult problems discussed in Section 2. This smoothing procedure is generalized in Section 4 for an arbitrary number of multiply connected substructures with non-conforming interfaces. In Section 5, we consider several substructure assembly problems arising in global/local analysis, heterogeneous designs, and coupled fluid/structure applications, and demonstrate the potential of the proposed smoothing procedure for improving the accuracy of the coupled analysis via Lagrange multipliers of independently modeled substructures. In Section 6, we comment on the merits of the ideas proposed in this paper, and finally in Section 7, we conclude this paper.

2. Background

2.1. A two-field hybrid method for the analysis of substructure problems

Let $\{\Omega^{(s)}\}_{s=1}^{s=N_s}$ denote a collection of substructures designed by different engineers, or obtained by 'tearing' a given structure into N_s pieces. In the former case, these substructures may have either matching or non-matching interfaces. In the latter case, they usually have compatible interfaces. In both cases, the objective is to construct the response of the global structure based on the independent analyses of the given substructures. This can be achieved using the two-field hybrid method described below for static analysis.

Solving a global elastostatic problem defined on the global structure $\Omega = \cup_{s=1}^{s=N_s} \Omega^{(s)}$ is equivalent to finding the displacement functions $\{u^{(s)}\}_{s=1}^{s=N_s}$ which are stationary points of the energy functionals

$$J^{(s)}(v^{(s)}) = \frac{1}{2} a(v^{(s)}, v^{(s)})_{\Omega^{(s)}} - (v^{(s)}, f)_{\Omega^{(s)}} - (v^{(s)}, h)_{\Gamma^{(s)}} \quad s = 1, 2, \ldots, N_s$$

where

$$\begin{aligned} a(v^{(s)}, w^{(s)})_{\Omega^{(s)}} &= \int_{\Omega^{(s)}} v^{(s)}_{(i,j)} c_{ijkl} w^{(s)}_{(k,l)} \, \mathrm{d}\Omega \\ (v^{(s)}, f)_{\Omega^{(s)}} &= \int_{\Omega^{(s)}} v_i^{(s)} f_i \, \mathrm{d}\Omega \, ; \qquad (v^{(s)}, h)_{\Gamma^{(s)}} = \int_{\Gamma_h^{(s)}} v_i^{(s)} h_i \, \mathrm{d}\Gamma \end{aligned} \tag{1}$$

and which satisfy on the global substructure interface boundary the continuity constraints

$$u^{(s)} = u^{(q)} \quad \text{on } \Gamma_I = \bigcup_{s=1,q=1}^{s=N_s,q=N_s} \{\overline{\Omega}^{(s)} \cap \overline{\Omega}^{(q)}\} \tag{2}$$

Here, the indices i, j, k take the value 1 to 3, $v_{(i,j)} = (v_{i,j} + v_{j,i})/2$ and $v_{i,j}$ denotes the partial derivative of the ith component of v with respect to the jth spatial variable, c_{ijkl} are the elastic coefficients, $\Gamma^{(s)}$ denotes the piecewise smooth boundary of substructure $\Omega^{(s)}$, and $\Gamma_h^{(s)}$ the piece of $\Gamma^{(s)}$ where the tractions h_i are prescribed.

Solving the N_s variational problems (1) with the subsidiary continuity conditions (2) is equivalent to finding the saddle-point of the two-field Lagrangian function

$$\mathscr{L}(v^{(1)}, v^{(2)}, \ldots, v^{(N_s)}, \mu^{(1)}, \mu^{(2)}, \ldots, \mu^{(t)}) = \sum_{s=1}^{s=N_s} J^{(s)}(v^{(s)}) + \sum_{s=1,q=1}^{s=N_s,q=N_s} (v^{(s)} - v^{(q)}, \mu^{(sq)})_{\Gamma_I}$$

where (3)

$$(v^{(s)} - v^{(q)}, \mu^{(sq)})_{\Gamma_I} = \int_{\Gamma_I} \mu^{(sq)} (v^{(s)} - v^{(q)}) \, \mathrm{d}\Gamma$$

that is, finding the displacement fields $\{u^{(s)}\}_{s=1}^{s=N_s}$ and the *interconnecting* Lagrange multipliers $\lambda^{(k)}$ (Fig. 2) that satisfy

$$\begin{aligned} \mathscr{L}(u^{(1)}, \ldots, u^{(N_s)}, \mu^{(1)}, \ldots, \mu^{(t)}) &\leq \mathscr{L}(u^{(1)}, \ldots, u^{(N_s)}, \lambda^{(1)}, \ldots, \lambda^{(t)}) \\ &\leq \mathscr{L}(v^{(1)}, \ldots, v^{(N_s)}, \lambda^{(1)}, \ldots, \lambda^{(t)}) \end{aligned} \tag{4}$$

for any admissible $\{v^{(s)}\}_{s=1}^{s=N_s}$ and $\{\mu^{(k)}\}_{k=1}^{k=t}$. The left inequality entails the interface continuity conditions, and the right inequality implies that among all admissible sets $\{v^{(s)}\}_{s=1}^{s=N_s}$ that satisfy the continuity conditions (2), the set $\{u^{(s)}\}_{s=1}^{s=N_s}$ minimizes the sum of the energy functionals $J^{(s)}$ defined on $\{\Omega^{(s)}\}_{s=1}^{s=N_s}$, respectively. Therefore, $\{u^{(s)}\}_{s=1}^{s=N_s}$ are the restriction of the solution u of the global structural problem to $\{\Omega^{(s)}\}_{s=1}^{s=N_s}$.

Now, if the substructure displacement fields and Lagrange multipliers are expressed by suitable shape functions as

$$u^{(s)} = N\hat{u}^{(s)} \qquad \lambda^{(s)} = \Lambda\hat{\lambda}^{(s)} \quad s = 1, 2, \ldots, N_s \tag{5}$$

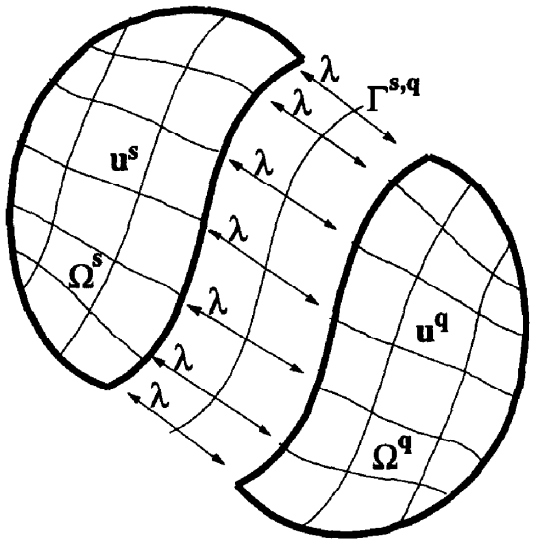

Fig. 2. A two-field hybrid method.

a standard Galerkin procedure transforms the two-field hybrid variational principle (4) into the constrained algebraic system

$$\begin{aligned} &K^{(s)}\hat{u}^{(s)} = \hat{f}^{(s)} - B^{(s)^{\mathrm{T}}}\hat{\lambda} \quad s = 1, 2, \ldots, N_s \\ &\sum_{s=1}^{s=N_s} B^{(s)}\hat{u}^{(s)} = 0 \end{aligned} \tag{6}$$

where $K^{(s)}$, $\hat{u}^{(s)}$ and $\hat{f}^{(s)}$ are respectively the stiffness matrix, the displacement vector, and the prescribed force vector associated with the finite element discretization of the substructure $\Omega^{(s)}$, and $B^{(s)}$, and $B^{(s)}$ enforces a weaker form of the continuity constraints (2) and is given by

$$B^{(s)} = \mathrm{sign}(\vec{n}^{(s)}) \int_{\Gamma^{(s)}} \Lambda^{\mathrm{T}} N \, \mathrm{d}\Gamma \tag{7}$$

where $\vec{n}^{(s)}$ is the normal at the interface boundary of $\Omega^{(s)}$. Clearly, $\hat{\lambda}$ denotes the vector of Lagrange multipliers and represents the forces needed for gluing together the substructures $\{\Omega^{(s)}\}_{s=1}^{s=N_s}$ along their boundary interface Γ_I.

An important issue for the above two-field hybrid method is the proper selection of the space of discretization of the Lagrange multipliers. In theory, the shape functions N and Λ must be constructed as to satisfy the Babuška–Brezzi condition. In practice, the Lagrange multipliers can be approximated using

- piece-wise constant or linear functions, in which case one recovers the mortar method [24]. This method is mathematically optimal, but cannot exploit a potential smoothness of the solution of a structural mechanics (elliptic) problem.
- polynomial functions. Away from cracks, interfaces between different materials and/or objects of different dimensions, the substructure displacement fields are usually smooth functions that can be glued together with a few Lagrange multipliers [16]. Hence, a two-field hybrid method with polynomial Lagrange multipliers can exploit a potential regularity of the solution of a structural mechanics problem, whereas the mortar method cannot. Clearly, a two-field hybrid method with polynomial Lagrange multipliers is also computationally more efficient than the mortar method, when the target substructure problem has large interfaces and the displacement field at these interfaces is not highly irregular.
- special polynomial functions, i.e. Chebyshev polynomials. In that case, the $B^{(s)}$ matrices and the algebraic system (6) are better conditioned than when the Lagrange multipliers are discretized with simple polynomials.

- piece-wise low-order polynomials as originally proposed in [16]. This choice of discretization is more difficult to implement than the polynomial option because it requires the generation of control and/or breaking points on the substructure interfaces. However, piece-wise low-order polynomials are a good alternative to high-order polynomials because they lead to better conditioned $B^{(s)}$ matrices and interface problems, and can be adapted to problems where the displacement solution is irregular on the substructure interfaces.

In any case, we note that the choice of a Lagrange multiplier polynomial or piece-wise polynomial order is not an easy one, especially when a low-dimensional discretization space is opted for. However, we also note that there exits theoretical results that guide the selection of polynomial Lagrange multipliers so that the corresponding two-field hybrid method satisfies the Babuška–Brezzi condition [28].

Previously, we have focused on developing flexible piece-wise polynomial discretizations of the interconnecting forces, and satisfying only a necessary condition implied by the Babuška–Brezzi theory. This necessary condition is the solvability—or non-singularity—of Eqs. (6). While such an approach is less than perfect from a mathematical viewpoint, it has allowed us to construct useful and powerful assembly and model reduction algorithms that we have successfully applied to the solution of complex structural problems [3,4,16,22].

REMARK 1. If the given substructures have matching interfaces and the continuity equations (2) are enforced for the discrete problem and at each interface degree of freedom (d.o.f.), $B^{(s)}$ becomes a boolean matrix that localizes a substructure quantity to its interface, and the functional spaces to which the solutions $u^{(s)}$ and $\lambda^{(s)}$ belong do not have to satisfy the Babuška–Brezzi condition. In that case, the first of Eqs. (6) correspond to the discrete equations of equilibrium of the substructure free-body diagrams, and the second of Eqs. (6) enforces a strong form of the continuity constraints (2).

REMARK 2. In the sequel, the hat superscript designating finite element vectors is dropped for simplicity. Hence, Eqs. (6) are re-written as

$$\begin{aligned} &K^{(s)}u^{(s)} = f^{(s)} - B^{(s)\mathrm{T}}\lambda \quad s = 1, 2, \ldots, N_s \\ &\sum_{s=1}^{s=N_s} B^{(s)}u^{(s)} = 0 \end{aligned} \tag{8}$$

When the substructures have matching interfaces, it is usually desirable to compute a displacement solution that is strongly continuous across the common interface boundary nodes. However, unless the continuity equations (2) are enforced for the discrete problem—that is, unless discrete Lagrange multipliers are introduced at the conforming interfaces—the displacement solution of Eqs. (8) will be in general discontinuous along Γ_I because Eqs. (3) enforce only a weak interface continuity. To address this problem, we have proposed in [16] a simple averaging procedure which, for a two-substructure homogeneous problem, consists in post-processing the computed substructure displacement fields as follows:

$$\tilde{u}^{(1)}|_{\Gamma_I} = \tilde{u}^{(2)}|_{\Gamma_I} = \tilde{u}_I = \frac{1}{2}(u^{(1)} + u^{(2)})|_{\Gamma_I} \tag{9}$$

In that case, we have also advocated back-propagating the effect of the above averaging procedure to the interior of each substructure, which implies the additional post-processing of each computed displacement field inside $\Omega^{(s)}$ by solving the displacement-driven problem

$$\begin{bmatrix} K_{ii}^{(s)} & K_{ib}^{(s)} \\ K_{ib}^{(s)\mathrm{T}} & K_{bb}^{(s)} \end{bmatrix} \begin{bmatrix} \tilde{u}_i^{(s)} \\ (u_b^{(s)} = \tilde{u}_I) \end{bmatrix} = \begin{bmatrix} f_i^{(s)} \\ g_b^{(s)} \end{bmatrix} \quad . \tag{10}$$

where the superscript T denotes the transpose of a matrix, the subscripts i and b designate the internal and interface boundary d.o.f., respectively, and $g_b^{(s)}$ is recovered during the solution of Eqs. (10). In [16], we have also advocated a similar averaging procedure for the case of non-matching substructure interfaces for accuracy improvement.

The post-processing procedure discussed above for conforming homogeneous substructures can be interpreted as a means for enforcing a posteriori a strong interface continuity between substructure displacement solutions

computed with an a priori weak interface continuity constraint. The objectives of this paper are: (a) to further motivate the need for such a post-processing procedure for heterogeneous substructure problems—that is, substructures with different material properties, and/or discrete resolutions, and/or geometric aspect ratios, (b) to extend the post-processing procedure previously proposed in [16] to problems with non-matching and heterogeneous substructures, and (c) to illustrate its potential for the coupled analysis of complex structural problems.

Next, we illustrate the two-field hybrid method summarized above with a simple example, and motivate the further developments presented in this paper.

2.2. Application to a two-substructure problem

Here, we consider the static analysis of an unsymmetric two-substructure ($\Omega^{(1)}$, $\Omega^{(2)}$) beam problem. Each substructure is clamped at one end, and the left one is subjected to a horizontal and vertical point loadings (Fig. 3). Both substructures are discretized using 4-node plane stress elements with two degrees of freedom per node and have matching discrete interfaces. Each finite element model contains 126 interior and 18 interface d.o.f.

In this problem, the substructures have matching interfaces. Therefore, they can be strongly glued together with discrete Lagrange multipliers introduced at each of the 18 interface d.o.f. When this option is chosen, we refer to the resulting displacement solution as the exact solution (u^{ex}), where 'exact' refers to the fact that Eqs. (8) deliver in that case a displacement field that is identical to that associated with the global (non-substructured) problem.

However, low-order polynomial Lagrange multipliers can also be used to enforce in a weaker sense the continuity conditions (2), and this is interesting for computational performance whenever accuracy can be preserved [16]. For example, Fig. 4 depicts the computed horizontal (u_{l_x}) and vertical (u_{l_y}) displacements along the interface boundary Γ_I when polynomials of degree $p = 0, 1, 2, 3$ are used to approximate the interface tractions. The reader can observe that:

- a second-order polynomial approximation of the Lagrange multipliers generates for this problem 6 interface unknowns only, and the corresponding averaged displacement solution is in excellent agreement with the exact solution that requires 18 interface unknowns.
- in all cases, the averaged substructure displacement solutions are more accurate than the non-averaged ones.

2.3. Effect of substructure heterogeneities

The averaging procedure outlined in Eq. (9) is justifiable only when the two substructures have roughly the same stiffness, which is unfortunately not true for all applications. Hence, the main objective of this paper is to generalize the smoothing procedure proposed in [16] to the case of arbitrary substructures. However, before

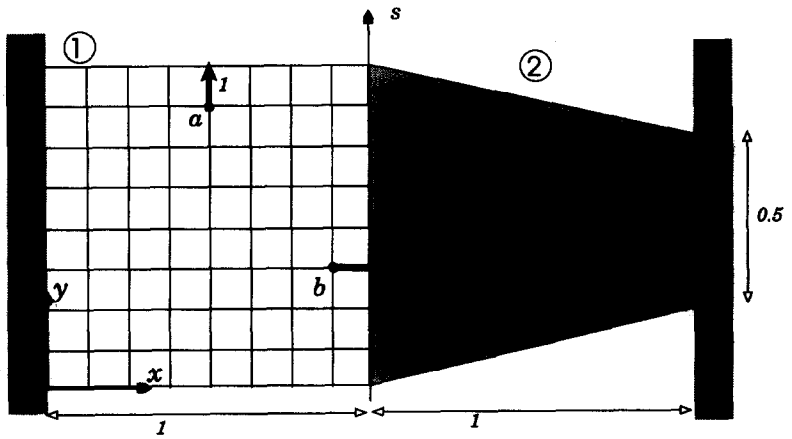

Fig. 3. Clamped–clamped unsymmetric two-substructure beam problem.

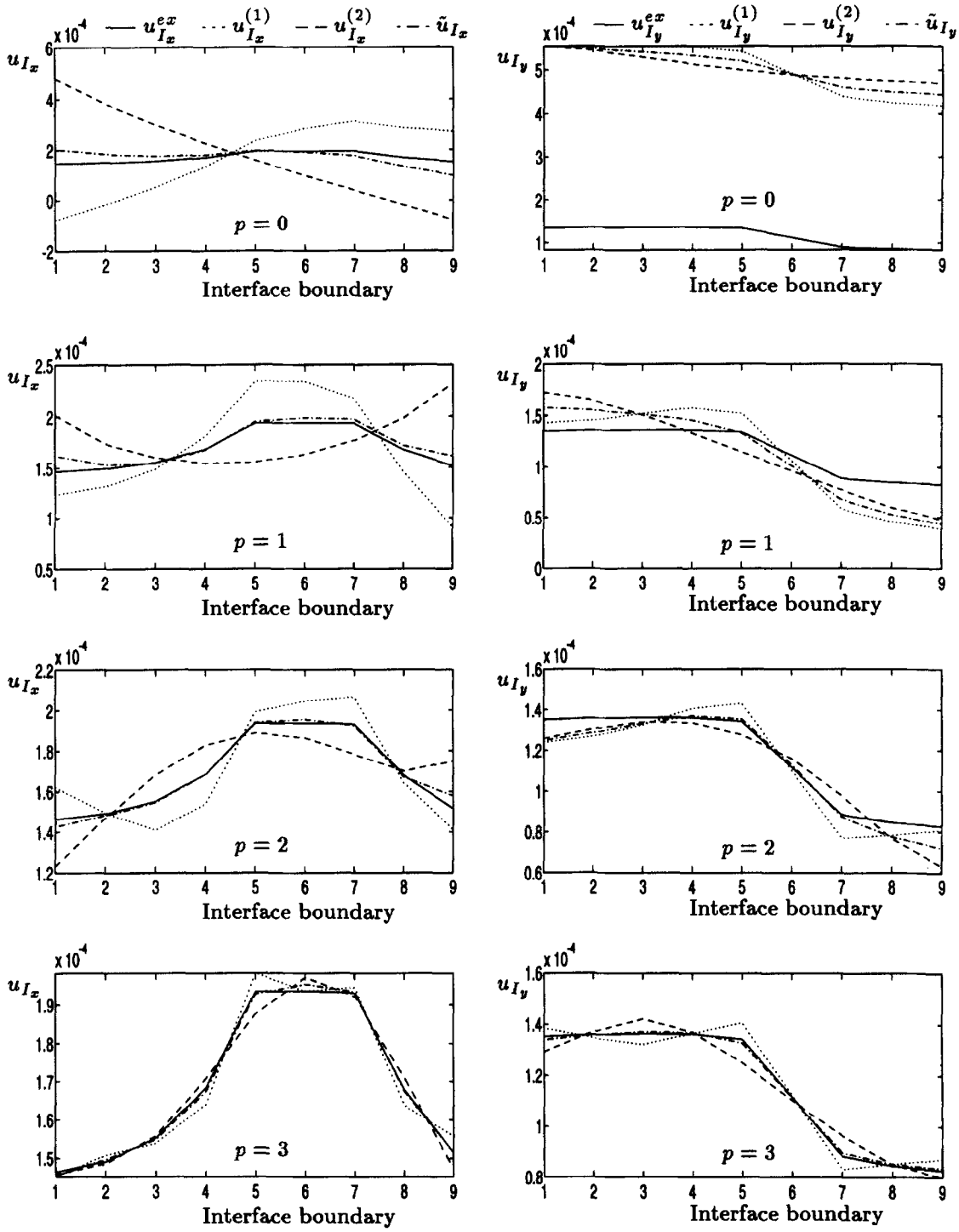

Fig. 4. Predicted horizontal and vertical interface displacement fields (homogeneous problem).

discussing such an extension, we begin with highlighting the effect of potential substructure heterogeneities on the accuracy of the displacement solutions computed by the two-field hybrid method.

For this purpose, we consider a modified version of the two-substructure problem described in Section 2.2, where the right substructure $\Omega^{(2)}$ is assumed to have a Young modulus equal to α times the value of that of the left substructure $\Omega^{(1)}$ ($\alpha = E^{(2)}/E^{(1)}$). We focus on second- and third-order polynomial approximations

($p = 2, 3$) of the Lagrange multipliers because these have been shown to produce excellent solutions in the homogeneous case $\alpha = 1$ (see Fig. 4). For all three values $\alpha = 1.0$, 0.4, 0.2, the horizontal and vertical substructure displacements are computed using the two-field hybrid method described in Section 2.1, and their traces on $\Gamma_I^{(1)}$ and $\Gamma_I^{(2)}$ are graphically depicted in Fig. 5 ($p = 2$) and Fig. 6 ($p = 3$).

For $\alpha = 1.0$—that is, for the case of a homogeneous two-substructure problem—the traces on $\Gamma_I^{(1)}$ and $\Gamma_I^{(2)}$ of the substructure displacements computed via the two-field hybrid method without any averaging procedure are shown to be nearly equally apart from the exact solution. For $\alpha \neq 1.0$—that is, for the case of a heterogeneous two-substructure problem—the trace on the interface boundary of the displacement field associated with the stiffer substructure is shown to be closer to the exact solution than that associated with the softer one. For $\alpha = 0.2$ and $p = 3$, the reader can observe that the computed interface displacement of the stiffer substructure is almost equal to the exact solution, while that of the softer substructure is far from it. Therefore, the simple averaging procedure (9) is clearly optimal in the homogeneous case, and suboptimal in the heterogeneous one. In this paper, we propose to devise an optimal smoothing procedure for improving the accuracy of the two-field hybrid method in the presence of various substructure heterogeneities.

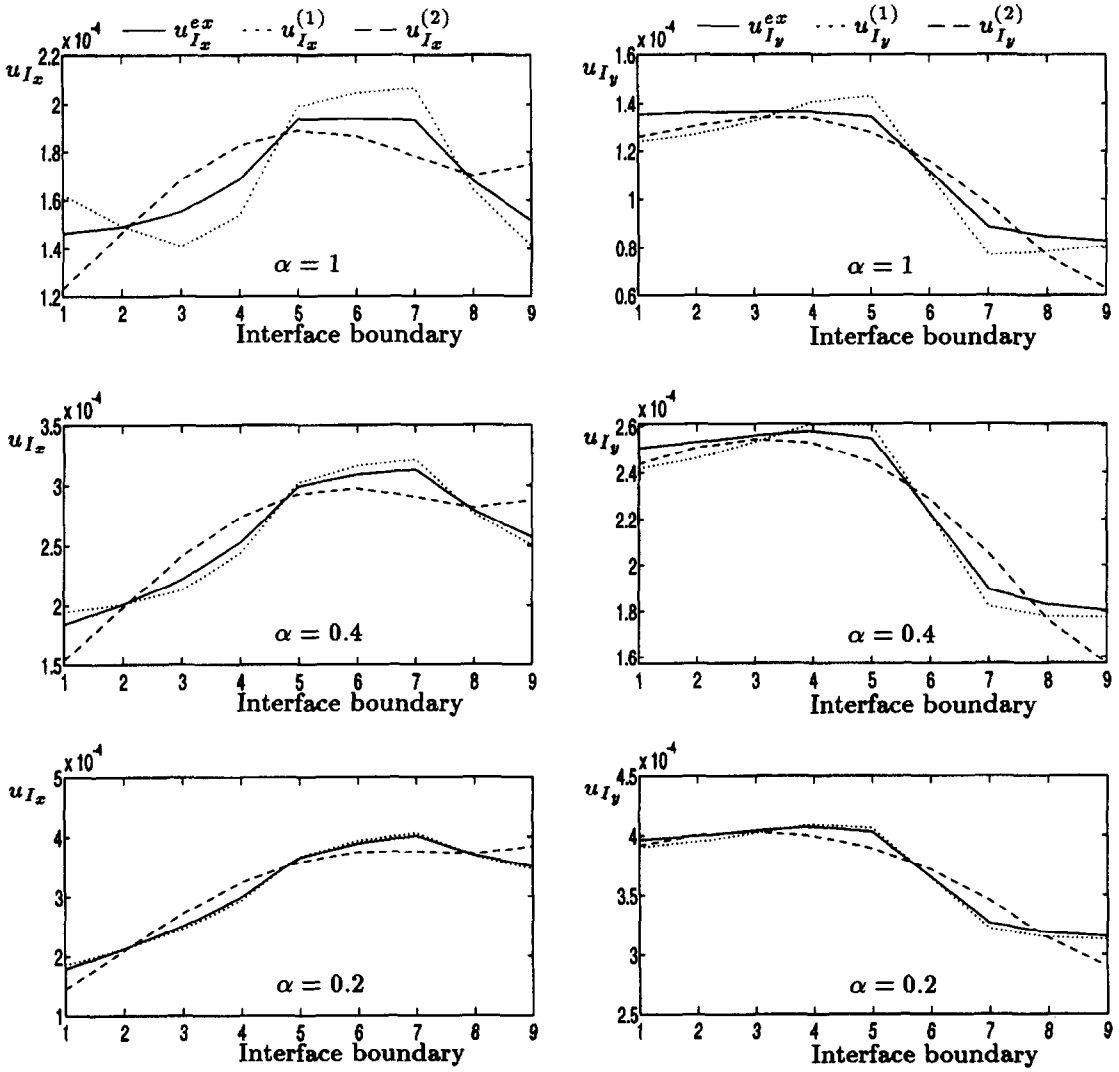

Fig. 5. Predicted horizontal and vertical interface displacement fields (heterogeneous problem—$p = 2$).

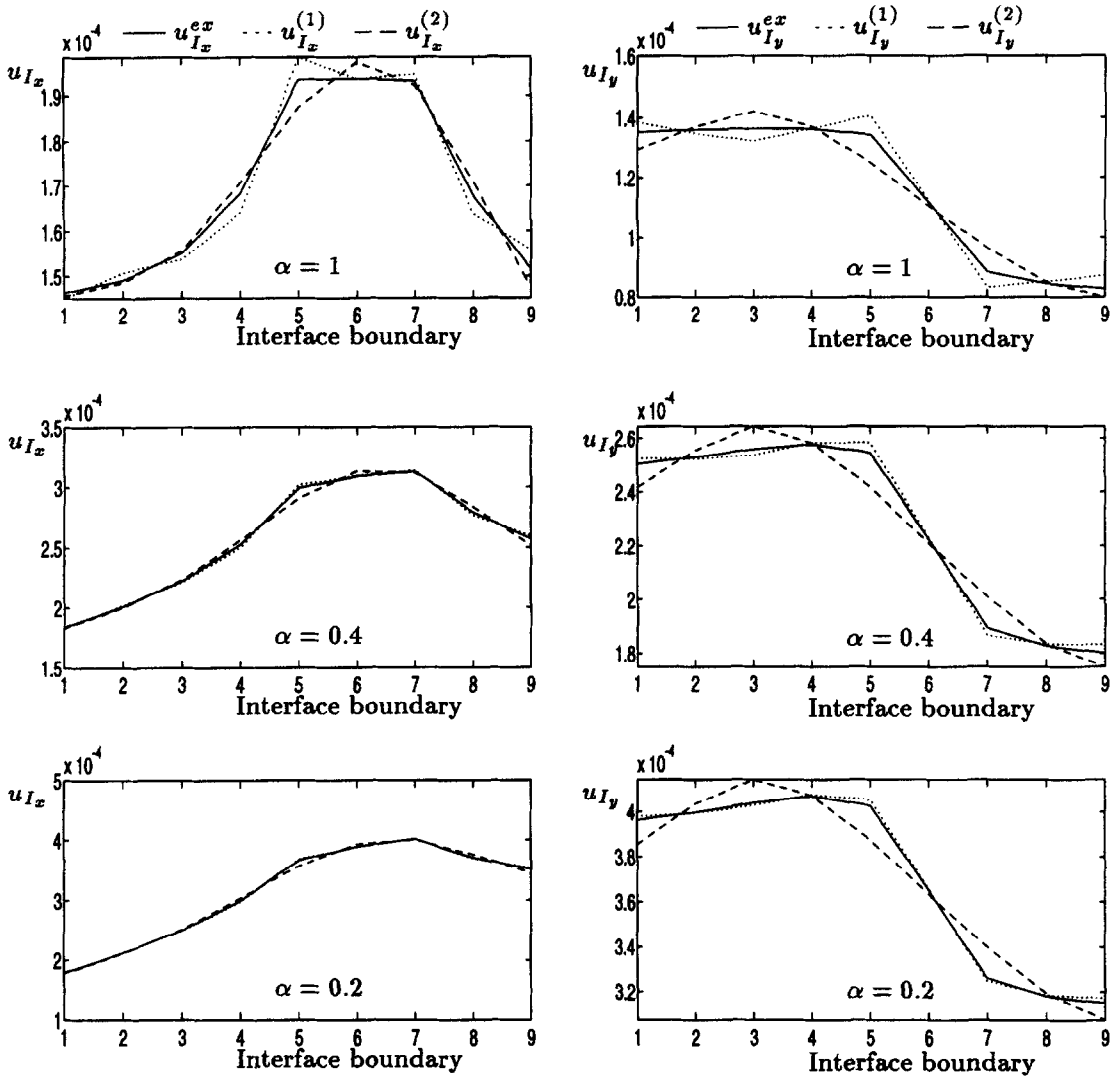

Fig. 6. Predicted horizontal and vertical interface displacement fields (heterogeneous problem—$p = 3$).

2.4. Parasitic eigenmodes and their effect on transient analysis

The two-field hybrid method can also be used for the dynamic analysis of complex substructure systems [2–4]. Here, we show numerically that even for homogeneous substructure problems, this method can introduce parasitic mode shapes when low-order approximations of the Lagrange multipliers are employed, which can significantly degrade the accuracy of the computed transient response of the system. Later in this paper, we will also show numerically that a suitable smoothing procedure can cure this problem too. For this purpose, we consider again the unsymmetric two-substructure homogeneous beam system introduced in Section 2.2 (Fig. 3). We use a first-order polynomial approximation of the Lagrange multipliers ($p = 1$) and compute the first 12 modes of the coupled system using a two-field eigensolver based on the dynamic equivalent of Eqs. (8) and described in [3]. Fig. 7 reports the obtained natural frequencies and compares them with the exact solution (frequencies of the non-substructured beam problem).

Even with $p = 1$, the two-field hybrid method is shown to deliver highly accurate frequencies for the first 7 modes. As one could have expected it, a degradation of accuracy is observed for the higher modes. However, it

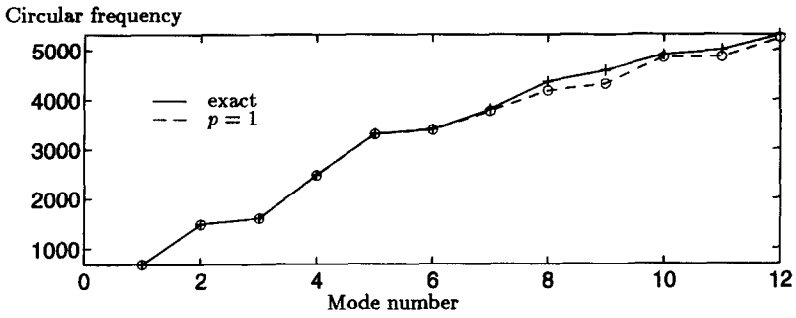

Fig. 7. First 12 natural frequencies of the unsymmetric beam system.

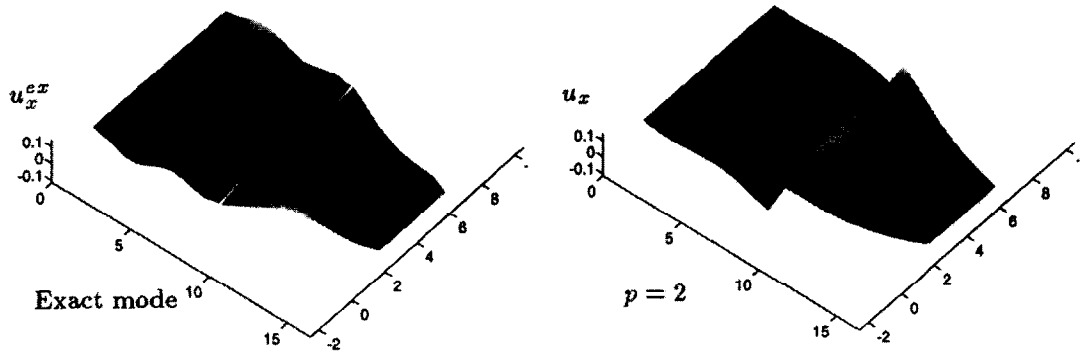

Fig. 8. Parasitic mode shape (eighth mode).

is particularly interesting to note that while the eighth frequency is computed with a relative error equal to 4.2×10^{-2}, the corresponding mode shape is not computed correctly (Fig. 8). We refer to such a discontinuous mode shape as a parasitic one.

The presence of such spurious modes can also be detected via their effect on the direct time-integration of the dynamic equivalent of the two-field hybrid Eqs. (8). Here, this is highlighted in Fig. 9 where the transient responses predicted by the trapezoidal rule using the two-field hybrid and the non-substructured equations of dynamic equilibrium are contrasted.

For the above problem, the inaccuracies exposed in the mode shape recovery and the transient response prediction can be attributed to the first-order approximation of the Lagrange multipliers, which is clearly not

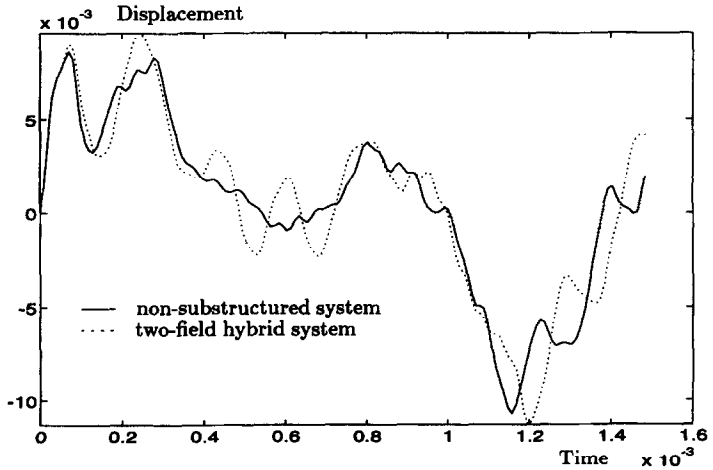

Fig. 9. Time-integration using the trapezoidal rule and $p = 1$.

sufficient in this case. However, we will show later that a smoothing procedure can be devised for improving the accuracy of the two-field hybrid method for transient computations, and that such a procedure is a better alternative than increasing the degree of the polynomial approximation of the Lagrange multipliers.

3. A Rayleigh–Ritz based smoothing procedure

In order not to obscure the main idea of this paper by the complexity of the notation needed for a problem with an arbitrary number of substructures with non-matching interfaces, we consider first the case of two heterogeneous substructures with conforming discrete interfaces. The general case of a system including multiply ($N_s > 2$) and arbitrarily connected substructures with non-matching interfaces is treated in Section 4.

3.1. From a statically admissible to a kinematically compatible system

Consider a two-substructure problem similar to that depicted in Fig. 3. Using the d.o.f. partitioning introduced in Eq. (10), Eqs. (8) can be re-written in this case as

$$\begin{bmatrix} K_{ii}^{(1)} & K_{ib}^{(1)} & 0 & 0 & 0 \\ K_{ib}^{(1)^{\mathrm{T}}} & K_{bb}^{(1)} & 0 & 0 & B^{(1)^{\mathrm{T}}} \\ 0 & 0 & K_{ii}^{(2)} & K_{ib}^{(2)} & 0 \\ 0 & 0 & K_{ib}^{(2)^{\mathrm{T}}} & K_{bb}^{(2)} & B^{(2)^{\mathrm{T}}} \\ 0 & B^{(1)} & 0 & B^{(2)} & 0 \end{bmatrix} \begin{bmatrix} u_i^{(1)} \\ u_b^{(1)} \\ u_i^{(2)} \\ u_b^{(2)} \\ \lambda \end{bmatrix} = \begin{bmatrix} f_i^{(1)} \\ f_b^{(1)} \\ f_i^{(2)} \\ f_b^{(2)} \\ 0 \end{bmatrix} \tag{11}$$

The post-processing procedure summarized in Eqs. (9)–(10) for two substructures sharing a matching interface can be generalized as follows:

$$\begin{aligned} &\tilde{u}_b^{(1)} = \tilde{u}_b^{(2)} = \tilde{u}_I = (1-a)u_b^{(1)} + a u_b^{(2)} \qquad 0 \leq a \leq 1 \\ &\tilde{u}_i^{(s)} = K_{ii}^{(s)^{-1}}(f_i^{(s)} - K_{ib}^{(s)}\tilde{u}_b^{(s)}) \\ &\quad = u_i^{(s)} - K_{ii}^{(s)^{-1}}K_{ib}^{(s)}(\tilde{u}_b^{(s)} - u_b^{(s)}) \qquad s = 1, 2 \end{aligned}$$

Here, a is a real number that is constant along the edge connecting the two substructures. Let δ_I denote the displacement jump on Γ_I defined as

$$\delta_I = u_b^{(2)} - u_b^{(1)} \tag{13}$$

From Eqs. (12)–(13), it follows that $\tilde{u}_b^{(1)}$ and $\tilde{u}_b^{(2)}$ can be re-written as

$$\begin{aligned} \tilde{u}_b^{(1)} &= u_b^{(1)} + \Delta u_b^{(1)} \\ \tilde{u}_b^{(2)} &= u_b^{(2)} + \Delta u_b^{(2)} \end{aligned} \tag{14}$$

where

$$\begin{aligned} \Delta u_b^{(1)} &= a\delta_I \\ \Delta u_b^{(2)} &= -(1-a)\delta_I \end{aligned} \tag{15}$$

Before discussing the optimal selection of the parameter a, we note that the smoothing procedure (12) destroys equilibrium while enforcing the desired strong compatibility on Γ_I. However, because the effect of the interface smoothing is back-propagated to the internal d.o.f. (see the second of Eqs. (12)), a force residual is introduced only on the interface Γ_I. Hence after post-processing, the substructure equations of equilibrium become

$$\begin{bmatrix} K_{ii}^{(1)} & K_{ib}^{(1)} & 0 \\ K_{ib}^{(1)^{\mathrm{T}}} & K_{bb}^{(1)} + K_{bb}^{(2)} & K_{ib}^{(2)} \\ 0 & K_{ii}^{(2)^{\mathrm{T}}} & K_{ii}^{(2)} \end{bmatrix} \begin{bmatrix} \tilde{u}_i^{(1)} \\ \tilde{u}_I \\ \tilde{u}_i^{(2)} \end{bmatrix} = \begin{bmatrix} f_i^{(1)} \\ f_b^{(1)} + f_b^{(2)} \\ f_i^{(2)} \end{bmatrix} + \begin{bmatrix} 0 \\ r_b \\ 0 \end{bmatrix} \tag{16}$$

From Eqs. (11) and (16), and after some algebraic manipulations, it follows that the interface residual caused by the proposed smoothing procedure can be written as

$$r_b = S_{bb}^{(1)} \Delta u_b^{(1)} + S_{bb}^{(2)} \Delta u_b^{(2)} \tag{17}$$

where $S_{bb}^{(s)}$ is the Schur-complement with respect to the interface boundary d.o.f. of the stiffness matrix of substructure $\Omega^{(s)}$

$$S_{bb}^{(s)} = K_{bb}^{(s)} - K_{ib}^{(s)^{\mathrm{T}}} K_{ii}^{(s)^{-1}} K_{ib}^{(s)} \tag{18}$$

Clearly, Eq. (17) shows that the interface residual r_b is directly related and only related to the displacement corrections resulting from enforcing a posteriori a strong compatibility on Γ_I. This residual can also be expressed in terms of the displacement jump δ_I as follows:

$$r_b = r_b(a) = (aS_{bb}^{(1)} + (a-1)S_{bb}^{(2)})\delta_I \tag{19}$$

In summary, after $u^{(1)}$ and $u^{(2)}$ have been obtained from the solution of Eqs. (8) that are associated with the two-field hybrid method (4), the jump δ_I is readily available, and the parameter a of the smoothing procedure (12) proposed for enforcing the desired strong compatibility along Γ_I should be selected as to minimize the undesired side-effect r_b.

3.2. Energy minimization

Rather than minimizing directly some norm of the interface residual r_b, we propose to adopt a Rayleigh–Ritz approach where the post-processed displacement solutions $\tilde{u}^{(1)}(a)$ and $\tilde{u}^{(2)}(a)$ given in Eqs. (12) are viewed as kinematically admissible fields parametrized by a, and minimize the corresponding energy of the global system. For the two-substructure problem discussed above, the total energy can be written as

$$\mathscr{E}(a) = \frac{1}{2} [\tilde{u}_i^{(1)^{\mathrm{T}}} \quad \tilde{u}_I^{\mathrm{T}} \quad \tilde{u}_i^{(2)^{\mathrm{T}}}] \begin{bmatrix} K_{ii}^{(1)} & K_{ib}^{(1)} & 0 \\ K_{ib}^{(1)^{\mathrm{T}}} & K_{bb}^{(1)} + K_{bb}^{(2)} & K_{ib}^{(2)} \\ 0 & K_{ib}^{(2)^{\mathrm{T}}} & K_{ii}^{(2)} \end{bmatrix} \begin{bmatrix} \tilde{u}_i^{(1)} \\ \tilde{u}_I \\ \tilde{u}_i^{(2)} \end{bmatrix} - [\tilde{u}_i^{(1)^{\mathrm{T}}} \quad \tilde{u}_I^{\mathrm{T}} \quad \tilde{u}_i^{(2)^{\mathrm{T}}}] \begin{bmatrix} f_i^{(1)} \\ f_b^{(1)} + f_b^{(2)} \\ f_i^{(2)} \end{bmatrix} \tag{20}$$

which, in view of Eq. (16) can also be expressed as

$$\mathscr{E}(a) = \frac{1}{2} [\tilde{u}_i^{(1)^{\mathrm{T}}} \quad \tilde{u}_I \quad \tilde{u}_i^{(2)^{\mathrm{T}}}] \begin{bmatrix} -f_i^{(1)} \\ -f_b^{(1)} - f_b^{(2)} + r_b \\ -f_i^{(2)} \end{bmatrix} \tag{21}$$

Using Eqs. (11), (12) and (21), we finally obtain

$$\mathscr{E}(a) = C - 2a\delta_I^{\mathrm{T}} S_{bb}^{(2)} \delta_I + a^2 \delta_I^{\mathrm{T}} (S_{bb}^{(1)} + S_{bb}^{(2)}) \delta_I \tag{22}$$

where C is an expression that does not depend on a. Differentiating $\mathscr{E}$ with respect to a, recalling Eq. (13), and enforcing the condition

$$\frac{\mathrm{d}\mathscr{E}}{\mathrm{d}a} = -2\delta_I^{\mathrm{T}} S_{bb}^{(2)} \delta_I + 2a\delta_I^{\mathrm{T}} (S_{bb}^{(1)} + S_{bb}^{(2)}) \delta_I = 0 \tag{23}$$

gives

$$\boxed{\begin{aligned} a &= \frac{k^{(2)}}{k^{(1)}+k^{(2)}} \\ k^{(1)} &= \delta_I^{\mathrm{T}} S_{bb}^{(1)} \delta_I = (u_b^{(2)} - u_b^{(1)})^{\mathrm{T}} S_{bb}^{(1)} (u_b^{(2)} - u_b^{(1)}) \\ k^{(2)} &= \delta_I^{\mathrm{T}} S_{bb}^{(2)} \delta_I = (u_b^{(2)} - u_b^{(1)})^{\mathrm{T}} S_{bb}^{(2)} (u_b^{(2)} - u_b^{(1)}) \end{aligned}} \tag{24}$$

Hence, from a physical viewpoint, the generalized smoothing (or averaging) procedure described by Eqs. (12) consists in treating the two substructures as two linear springs in series, computing the displacement jump at their point of connection, and redistributing this jump among both springs according to their 'relative stiffnesses' $k^{(1)}$ and $k^{(2)}$. Such a procedure was previously suggested in [11] within the context of the FETI (Finite Element Tearing and Interconnecting) method [1,9,11,19] and its preconditioned conjugate gradient solver. However, Eqs. (24) give for the first time rational values of the substructure spring constants $k^{(1)}$ and $k^{(2)}$ that clearly contain the effect of material properties and mesh resolution. These constants can be described as the Schur-complement norms of the displacement jump at the substructure interfaces.

REMARK 3. The Schur-complement matrices $S_{bb}^{(s)}$ do not need to be explicitly computed. Only their action on the displacement jump vector should be evaluated [11].

REMARK 4. If the two substructures and their finite element models are identical, from Eqs. (24) it follows that $k^{(1)} = k^{(2)}$ and $a = 1/2$, which shows that the generalized smoothing procedure defined by Eqs. (12), (24) includes the averaging scheme (9) as a particular case.

REMARK 5. As stated before, a is chosen here to be constant along the edge Γ_I. However, one could also discretize a in some nontrivial polynomial space, or ultimately, introduce a different smoothing parameter a for each interface d.o.f. Such alternative strategies can only be more accurate but are surely computationally more expensive than the present one. (If the given substructures have conforming interfaces and a smoothing parameter is introduced at each interface d.o.f., the two-field hybrid method recovers the exact solution.) Nevertheless, we recommend using three different constant smoothing parameters a_x, a_y and a_z for the three different directional components u_{I_x}, u_{I_y} and u_{I_z} of the interface displacement field, especially when the stiffness of the interface problem varies significantly from one direction to another.

Finally, it is worthwhile noting that

$$\begin{aligned} \delta_I^{\mathrm{T}} r_b &= \delta_I^{\mathrm{T}} (a S_{bb}^{(1)} + (a-1) S_{bb}^{(2)}) \delta_I \\ &= \delta_I^{\mathrm{T}} \frac{k^{(2)} S_{bb}^{(1)} - k^{(1)} S_{bb}^{(2)}}{k^{(1)}+k^{(2)}} \delta_I \\ &= \frac{(\delta_I^{\mathrm{T}} S_{bb}^{(1)} \delta_I)(\delta_I^{\mathrm{T}} S_{bb}^{(2)} \delta_I) - (\delta_I^{\mathrm{T}} S_{bb}^{(1)} \delta_I)(\delta_I^{\mathrm{T}} S_{bb}^{(2)} \delta_I)}{\delta_I^{\mathrm{T}} (S_{bb}^{(1)} + S_{bb}^{(2)}) \delta_I} \\ &= 0 \end{aligned} \tag{25}$$

which

- stresses the fact that the smoothing procedure described in Eqs. (12) is equivalent to a Rayleigh–Ritz method where the displacement shape functions are governed by the parameter a.
- shows that the dual quantities (residual interface loads introduced by the proposed smoothing procedure, displacement corrections) do not produce work.

3.3. Accuracy improvement

In order to illustrate the beneficial effects of the proposed smoothing procedure, we consider first the

heterogeneous two-substructure problem discussed in Section 2.3, apply the two-field hybrid method, and post-process the computed substructure displacements using formulae (12), (24). The obtained results are summarized in Figs. 10 and 11 for $\alpha = 1.0$, 0.4, 0.2 and $p = 2, 3$. For comparison purposes, we have also included in these figures the results computed in Section 2.3.

Clearly, the results reported in Figs. 10 and 11 show that, unlike the original results obtained by the two-field hybrid method (Figs. 5 and 6), the smoothed horizontal and vertical interface displacement fields are in perfect agreement with the exact solution, which demonstrates the importance of the generalized averaging procedure (12) for heterogeneous substructure problems.

Moreover, it appears that, for a given p, the more heterogeneous the substructure problem is, the more accurate the smoothed two-field hybrid solution is. This statement is well-supported by Fig. 12 which depicts the relative error $(u_I^{\text{exact}}(i) - \tilde{u}_I(i))/u_I^{\text{exact}}(i)$ for each ith horizontal and vertical interface d.o.f. The results reported in Fig. 12 also suggest that for a chosen level of accuracy, a lower p is needed for a higher degree of heterogeneity when the smoothing procedure (12) is employed.

Next, we consider again the unsymmetric two-substructure dynamic problem described in Section 2.4. We use

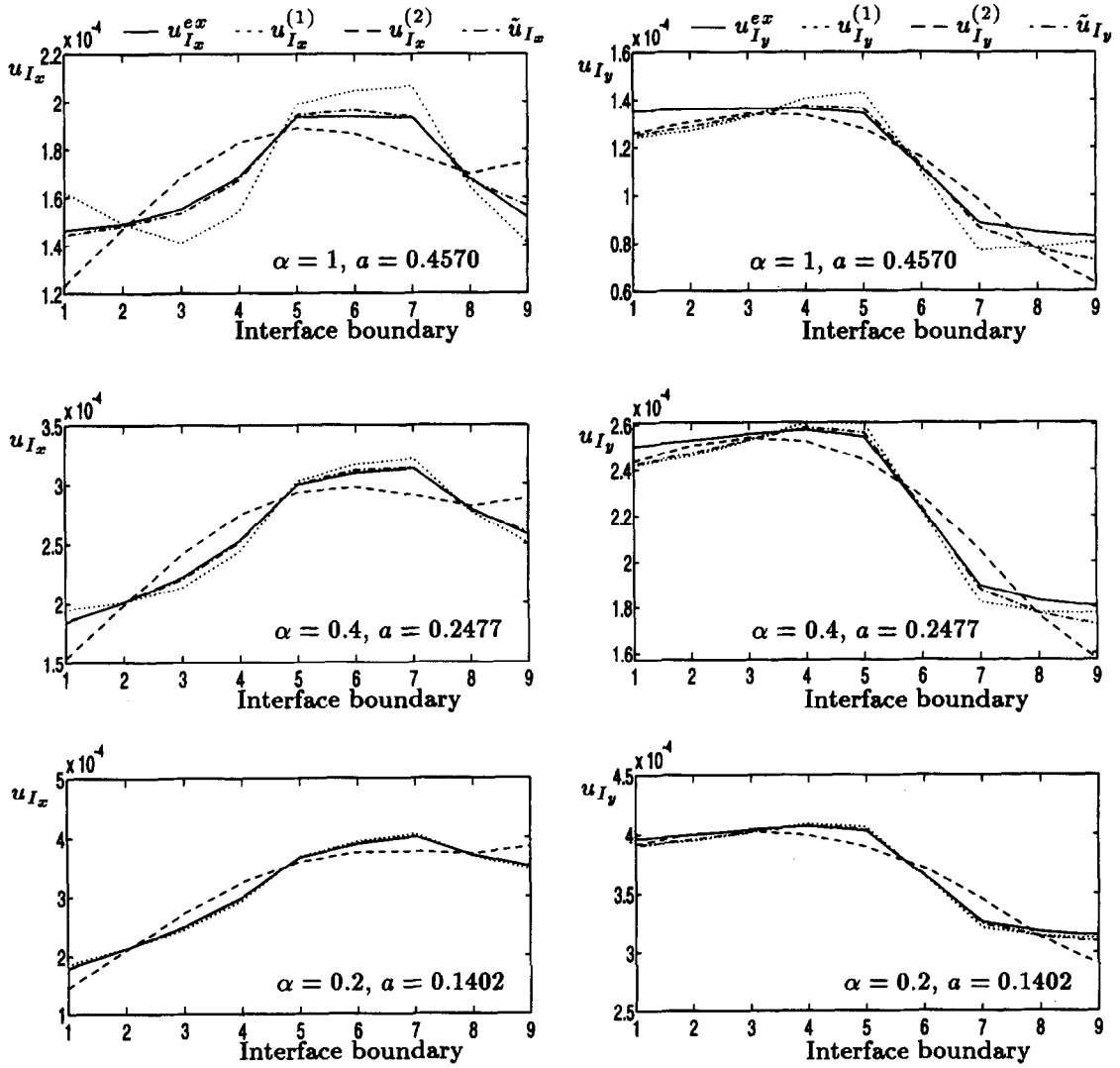

Fig. 10. Smoothed horizontal and vertical interface displacement fields (heterogeneous problem—$p = 2$).

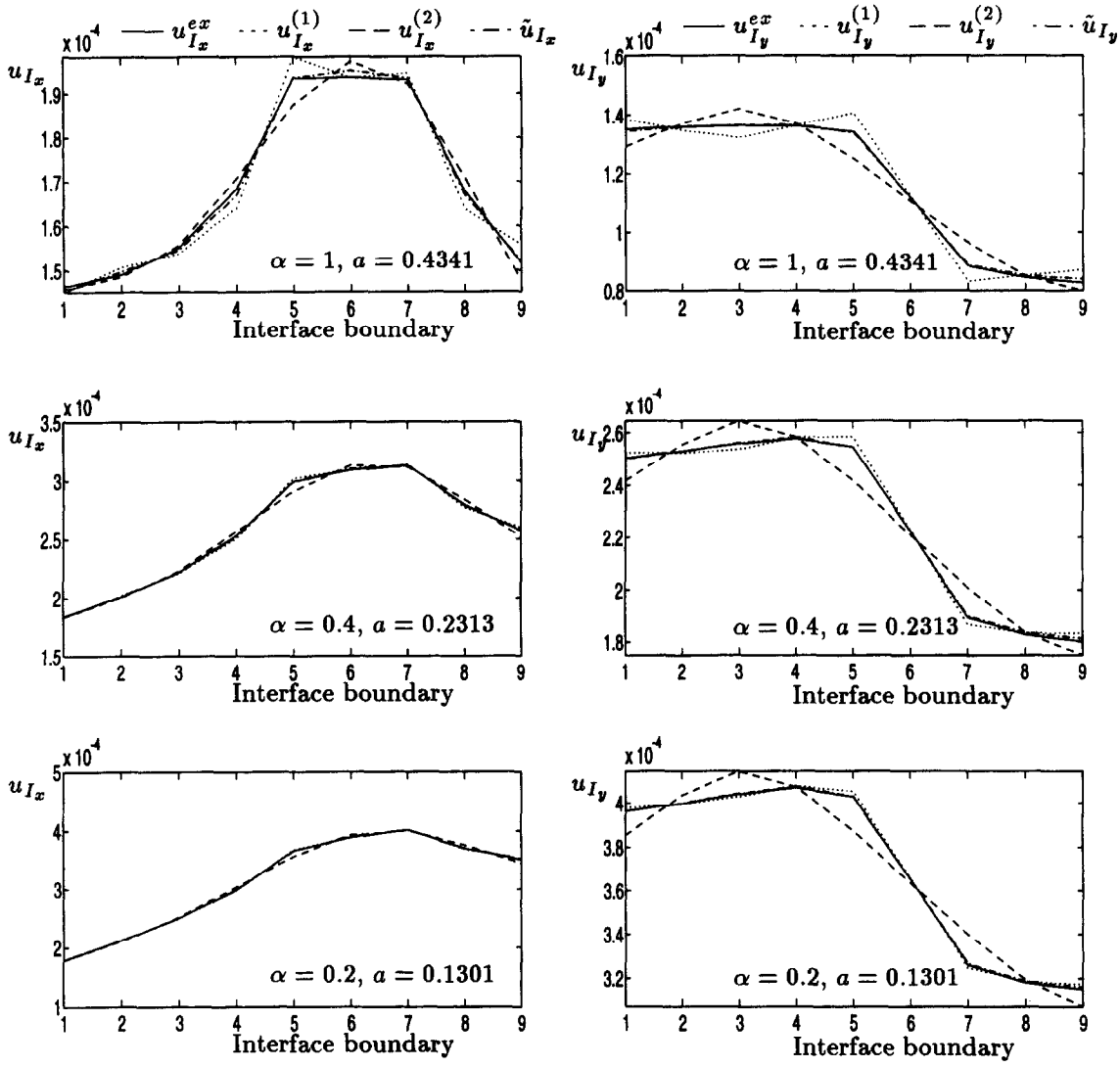

Fig. 11. Smoothed horizontal and vertical interface displacement fields (heterogeneous problem—$p = 3$).

the trapezoidal rule to integrate the non-substructured as well as the two-field hybrid ($p = 1$) equations of dynamic equilibrium. In Fig. 13 we report the so-called exact solution, and the results obtained for the two-field hybrid method with and without smoothing. Note that for dynamic problems, the smoothing procedure (12) is applied at each time-step. From the comparison with the results reported in Fig. 9, smoothing is clearly shown to significantly improve the accuracy of the transient two-field hybrid computations.

3.4. An economical alternative for repeated problems

When smoothing is required repetitively as in transient problems, it becomes interesting to consider a 'cheaper' variant of procedure (12) where the effect of the interface smoothing is not back-propagated to the internal d.o.f. Following a derivation that is similar to that presented in Section 3.2, the reader can check that such a strategy leads to a smoothing procedure that is similar to that described in Eqs. (12) but where the Schur-complement matrices $S^{(s)}_{bb}$ are replaced by the 'lumped' [11] interface stiffness matrices $K^{(s)}_{bb}$.

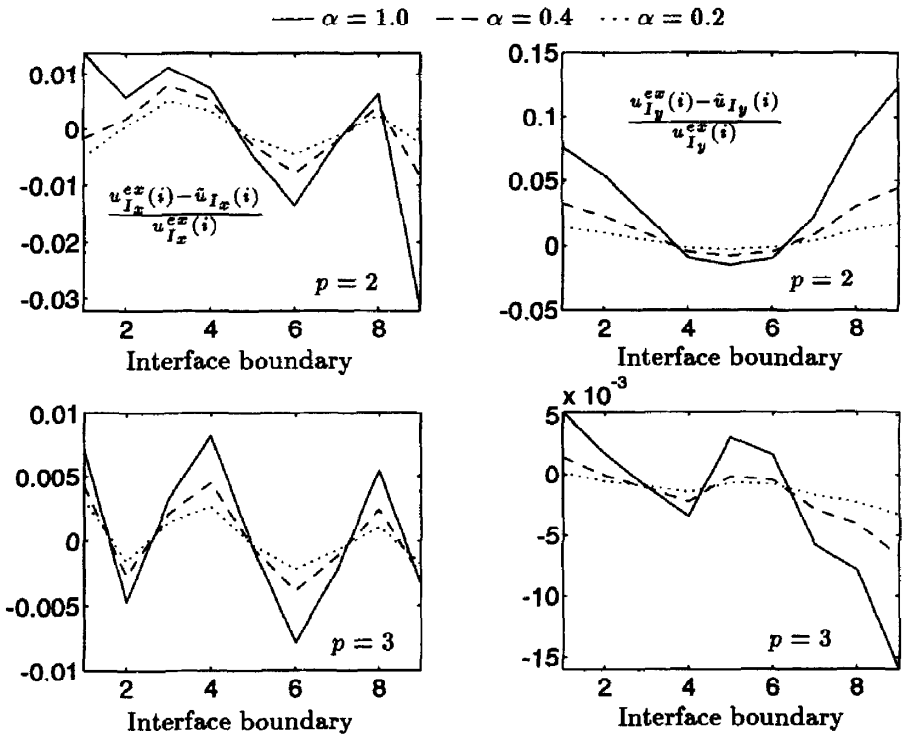

Fig. 12. Relative errors ($p = 2$ and $p = 3$).

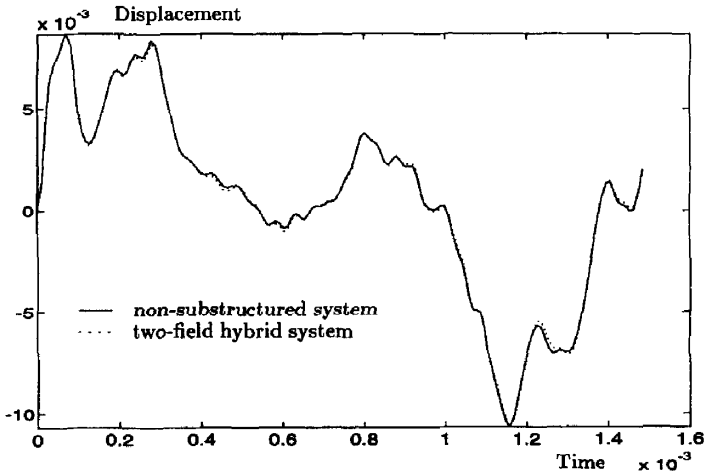

Fig. 13. Effect of smoothing on time-integration using the trapezoidal rule and $p = 1$.

$$
\begin{aligned}
a^{\mathrm{L}} &= \frac{k^{(2)^{\mathrm{L}}}}{k^{(1)^{\mathrm{L}}} + k^{(2)^{\mathrm{L}}}} \\
k^{(1)^{\mathrm{L}}} &= \delta_l^{\mathrm{T}} K_{bb}^{(1)} \delta_l = (u_b^{(2)} - u_b^{(1)})^{\mathrm{T}} K_{bb}^{(1)} (u_b^{(2)} - u_b^{(1)}) \\
k^{(2)^{\mathrm{L}}} &= \delta_l^{\mathrm{T}} K_{bb}^{(2)} \delta_l = (u_b^{(2)} - u_b^{(1)})^{\mathrm{T}} K_{bb}^{(2)} (u_b^{(2)} - u_b^{(1)})
\end{aligned}
\tag{26}
$$

The computational advantages of the above lumped strategy are obvious given that K_{bb} is readily available and

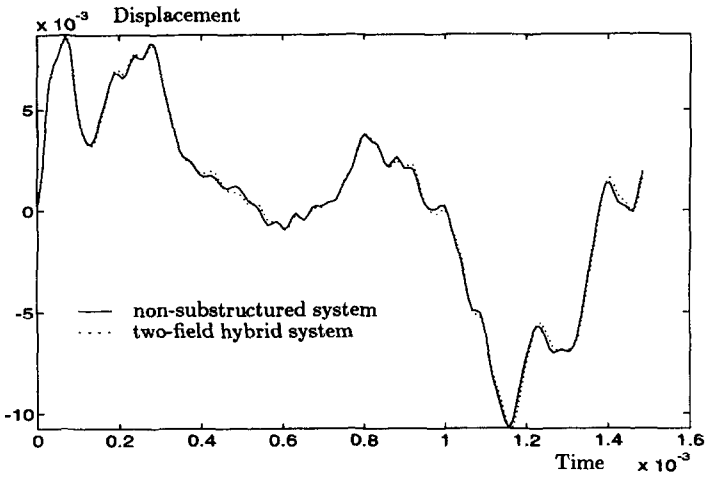

Fig. 14. Time-integration using the trapezoidal rule and $p = 1$. Lumped smoothing procedure.

only simple matrix–vector multiplications are needed to evaluate the lumped averaging parameter a^L. Moreover, it is our experience that for practical time-steps, smoothing with the lumped strategy (26) retains almost the same order of accuracy as smoothing with the less economical but complete procedure (12). This is illustrated in Fig. 14 for the two-substructure dynamic problem introduced in Section 2.4.

4. Assembly of multiple conforming and non-conforming substructures

When the given substructures have non-matching discrete interfaces, the issue of strong (discrete) continuity on Γ_I does not arise because in that case the substructure displacement fields are not necessarily computed on the same physical interface nodes. However, we will show that even in that case, smoothing is beneficial and can be interpreted as a means for enforcing a posteriori an interface continuity between the substructure displacements that is stronger than that resulting from the solutions generated by the two-field hybrid method. For example, if the Lagrange multipliers needed for enforcing the continuity constraints (2) across a certain interface are approximated with a pth order polynomial, the substructure displacement fields computed by the two-field method can be post-processed to satisfy $\int_{\Gamma_I} \mu^{(sq)}(v^{(s)} - v^{(q)})\, d\Gamma = 0$, where $\mu^{(sq)}$ is approximated by a qth order polynomial with $q > p$. In the sequel, we refer to this post-processing paradigm as a qth order smoothing procedure.

REMARK 6. The qth order smoothing concept discussed here is equally applicable when the Lagrange multipliers are approximated with piece-wise polynomials as in [1,4,16] rather than polynomials.

4.1. Conventions and mathematical preliminaries

Let $b^{(s)}$ denote the restriction of the operator $B^{(s)}$ defined in Eq. (7) to the interface boundary $\Gamma_I^{(s)}$ of a given substructure $\Omega^{(s)}$. From the partitioning and numbering conventions implied by Eqs. (10), we have

$$B^{(s)} = [0 \quad b^{(s)}] \tag{27}$$

The interface boundary of each substructure can be broken into *edges*. Here, an edge is defined as the collection of *all* neighboring interface nodes that are shared by the *same group of substructures*, and each substructure interface node is assigned to *one and only one* substructure edge. Note that this definition is independent from the dimensionality of the interface (Fig. 15). Consequently, the traditional crosspoint that is often referred to in the domain decomposition literature as a 'vertex' for two-dimensional problems is treated

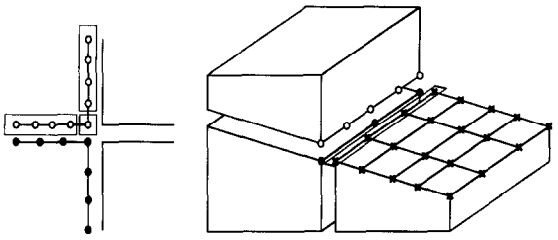

Fig. 15. Edges and crosspoints for two- and three-dimensional substructure problems.

here as an edge with a single interface node (Fig. 15). For three-dimensional problems, the crosspoint is an edge with an arbitrary number of interface nodes. It follows that $b^{(s)}$ can be partitioned as

$$b^{(s)} = [b^{(s),i} \quad b^{(s),j} \quad \cdots \quad b^{(s),l}] \tag{28}$$

where $b^{(s),j}$ is the restriction of $b^{(s)}$ to the jth edge of $\Gamma_I^{(s)}$. Usually, the continuity constraints across an edge j are enforced independently from those across and edge $j \neq l$, and therefore one has

$$b^{(s),j^{\mathrm{T}}} b^{(s),l} = 0 \tag{29}$$

Moreover, an edge j can be shared by multiple substructures, and therefore $b^{(s),j}$ can also be partitioned as

$$b^{(s),j} = \begin{bmatrix} 0 \\ \vdots \\ b^{(s,q),j} \\ 0 \\ b^{(s,r),j} \\ \vdots \\ 0 \end{bmatrix} \tag{30}$$

where $b^{(s,q),j}$ is the component of $b^{(s),j}$ pertaining to the interconnectivity of substructures $\Omega^{(s)}$ and $\Omega^{(q)}$ along edge j.

Next, we define the multiplicity m_i of an edge i as the number of substructures it interconnects. Hence, $m_i \geq 2$, and for a crosspoint $m_i > 2$. In particular, we note that for conforming interfaces, the following holds

$$b^{(s,q),j^{\mathrm{T}}} b^{(s,q),j} = I; \qquad b^{(s),j^{\mathrm{T}}} b^{(s),j} = (m_i - 1)I \tag{31}$$

Finally, we introduce the unsigned equivalents of $B^{(s)}$, $b^{(s)}$, $b^{(s),j}$ and $b^{(s,q),j}$, and designate them with a hat superscript. For example, we have

$$\hat{b}^{(s,q),j} = \int_{\Gamma^{(s,q),j}} \Lambda^{\mathrm{T}} N \, \mathrm{d}\Gamma$$

We assume that along an edge i, the same approximation is used for the Lagrange multipliers interconnecting any pair of substructures $\Omega^{(s)}$ and $\Omega^{(q)}$. To emphasize this point, we use in the sequel the notation $b^{(s,-),j}$ rather than $b^{(s,q),j}$.

Using the above definitions and notation, it follows that the compatibility equations between the substructure interfaces can be written in the general case as

$$\hat{b}^{(s,-),j} u_b^{(s),j} - \hat{b}^{(r,-),j} u_b^{(r),j} = 0 \quad \forall j, \quad \forall \Gamma_I^{(s,r)} \ni j \tag{32}$$

where $u_b^{(s),j}$ is the trace of the displacement field on the substructure edge $\Gamma_I^{(s),j}$.

In order to satisfy the Babuška–Brezzi condition, we assume that the degree p of the polynomial approximation of the Lagrange multiplier interconnecting two substructures $\Omega^{(s)}$ and $\Omega^{(q)}$ is smaller than the square root of the local size of the coarsest discretization of the interface $\Gamma_I^{(s,q)}$ [28]. In that case, $\hat{b}^{(s,-),j}$ is a rectangular matrix with fewer rows than columns, $\hat{b}^{*(s,-),j}$ denotes its null space

$$\hat{b}^{(a,-),j}\hat{b}^{*(s,-),j} = 0 \tag{33}$$

and the matrix product $[\hat{b}^{(s,-),j}\hat{b}^{*(s,-),j^{\mathrm{T}}}]$ is non-singular. Lastly, following the spirit of the FETI method [9,11] we decompose any vector x into a component residing in the null space of $\hat{b}^{(s,-),j}$, and a component belonging to the range of its transpose

$$\begin{aligned} x &= B^{(s,-),j}y + \hat{b}^{*(s,-),j}z \\ B^{(s,-),j} &= \hat{b}^{(s,-),j^{\mathrm{T}}}[\hat{b}^{(s,-),j}\hat{b}^{(s,-),j^{\mathrm{T}}}]^{-1} \end{aligned} \tag{34}$$

In particular, we note that

$$\begin{aligned} y &= \hat{b}^{(s,-),j}x \\ z &= [\hat{b}^{*(s,-),j^{\mathrm{T}}}\hat{b}^{*(s,-),j}]^{-1}\hat{b}^{*(s,-),j^{\mathrm{T}}}x \end{aligned} \tag{35}$$

REMARK 7. In the particular case of substructures with matching interfaces, we have $\hat{b}^{*(s,-),j} = 0$ and $\hat{b}^{(s,-),j}\hat{b}^{(s,-),j^{\mathrm{T}}} = I$.

4.2. The generalized smoothing procedure

If the Lagrange multipliers needed for enforcing the continuity constraints (2) across an edge $\Gamma_l^{(s,t),j}$ are approximated with a pth order polynomial, the substructure displacement fields computed using the two-field method will satisfy

$$\hat{b}_p^{(s,-),j}u_b^{(s),j} - \hat{b}_p^{(t,-),j}u_b^{(t),j} = 0 \tag{36}$$

In Eq. (36) above, the subscript p is used to emphasize the dependence of $b^{(s,-),j}$ and $b^{(t,-),j}$ on the pth order polynomial approximation. However, if $b_q^{(s,-),j}$ is the constraint matrix associated with a qth order polynomial approximation of the Lagrange multipliers and $q > p$, the computed substructure displacement fields using a pth order approximation of the Lagrange multipliers will satisfy

$$\hat{b}_q^{(s,-),j}u_b^{(s),j} - \hat{b}_q^{(t,-),j}u_b^{(t),j} = r_q^{(s,t),j} \neq 0 \tag{37}$$

where $r_q^{(s,t),j}$ can be interpreted as a compatibility residual along the edge $\Gamma_l^{(s,t),j}$. It becomes therefore clear that for substructure problems with non-matching interfaces, the objective of a qth order generalized smoothing procedure (see the introduction of Section 4) is to drive the compatibility residual $r_q^{(s,t),j}$ to zero—that is, to compute substructure displacement fields $\tilde{u}_b^{(s),j}$ and $\tilde{u}_b^{(t),j}$ that are compatible with respect to a higher-order weighting matrix than the one used for enforcing equilibrium (or with respect to the boolean matrix $B^{(s)}$ in the case of compatible interfaces)

$$\hat{b}_q^{(s,-),j}\tilde{u}_b^{(s),j} - \hat{b}_q^{(t,-),j}\tilde{u}_b^{(t),j} = 0 \tag{38}$$

In the sequel, we drop the p and q subscripts for simplicity.

First, we note that because the same approximation is used for the Lagrange multipliers interconnecting any pair of substructures $\Omega^{(s)}$ and $\Omega^{(q)}$ (see Section 4.1), the subvector of Lagrange multipliers associated with an edge i has the same size in all the substructures where it is evaluated. Therefore, one can construct the edge field ν^j defined as

$$\nu^j = \sum_{\Gamma_l^{(s)} \ni j} \beta^{(s),j}\hat{b}^{(s,-),j}u_b^{(s),j} \tag{39}$$

where the real coefficients $\beta^{(s),j}$ will play the same role as the averaging parameter a introduced in the first of Eqs. (12). Clearly, for any combination of $\beta^{(s),j}, \nu^j$ is not specific to any substructure connected to edge i. Hence, it is a prime candidate for constructing a smoothed substructure displacement field $\tilde{u}_b^{(s),j}$ that verifies the stronger compatibility equations (38). Using the decomposition (34) and focusing on satisfying Eq. (38), we

impose that the component of $\tilde{u}_b^{(s),j}$ residing in the range of $\hat{b}^{(s,-),j^T}$ be equal to ν^j, and that the one belonging to $\hat{b}*^{(s,-),j}$ be the same as that obtained from the decomposition of $u_b^{(s),j}$

$$\begin{aligned} \tilde{u}_b^{(s),j} &= B^{(s,-),j}\nu^j + \hat{b}*^{(s,-),j}\mu^j \\ \mu^j &= [\hat{b}*^{(s,-),j^T}\hat{b}*^{(s,-),j}]^{-1}\hat{b}*^{(s,-),j^T}u_b^{(s),j} \end{aligned} \tag{40}$$

Using Eq. (33), the reader can easily verify that the proposed smoothed substructure displacement $\tilde{u}_b^{(s),j}$ verifies the objective compatibility equations (38). Finally, from Eqs. (39), (40) and the principle of back-propagation introduced in Section 2.1, it follows that the generalized smoothing procedure can be written for an arbitrary substructure problem as

$$\boxed{\begin{aligned} \tilde{u}_b^{(s),j} &= \sum_{\Gamma_I^{(t)} \ni j} \beta^{(t),j} B^{(s,-),j} \hat{b}^{(t,-),j} u_b^{(t),j} + \hat{b}*^{(s,-),j}\mu^j \\ \tilde{u}_i^{(s)} &= -K_{ii}^{(s)^{-1}} K_{ib}^{(s)} \Delta u_b^{(s)} + u_i^{(s)} \end{aligned}} \tag{41}$$

It remains to find the optimal values of the coefficients $\beta^{(s),j}$. For this purpose, we follow conceptually the same Rayleigh–Ritz approach that was presented in Section 3.2.

4.3. Energy minimization

Let $\Delta u_b^{(s),j}$ be defined as

$$\Delta u_b^{(s),j} = \tilde{u}_b^{(s),j} - u_b^{(s),j} \tag{42}$$

If the coefficients $\beta^{(s),j}$ are constrained to have a unit sum

$$\boxed{\sum_{\Gamma_I^{(s)} \ni j} \beta^{(s),j} = 1} \tag{43}$$

then from Eqs. (40)–(42) it follows that

$$\Delta u_b^{(s),j} = -\sum_{\Gamma_I^{(t)} \ni j, t \neq s} \beta^{(t),j} B^{(s,-),j} r^{(s,t)j} \tag{44}$$

In the particular case of conforming interfaces, the above expression simplifies to

$$\Delta u_b^{(s),j} = -\hat{b}^{(s,-),j^T} \sum_{\Gamma_I^{(t)} \ni j, t \neq s} \beta^{(t),j} r^{(s,t),j} \tag{45}$$

For an arbitrary substructure problem, the total energy can be written as

$$\mathscr{E}(\beta^{(s),j}) = \sum_{s=1}^{s=N_s} \tilde{u}^{(s)^T} K^{(s)} \tilde{u}^{(s)} - \tilde{u}^{(s)^T} f^{(s)} \tag{46}$$

If the effect of interface smoothing is back-propagated to the substructure interiors, $\mathscr{E}(\beta^{(s),j})$ can be re-written after using Eqs. (11), (41), (42) as

$$\mathscr{E}(\beta^{(s),j}) = \sum_{s=1}^{s=N_s} \tilde{u}_b^{(s)^T} S_{bb}^{(s)} \tilde{u}_b^{(s)} - \tilde{u}_b^{(s)^T} (f_b^{(s)} - K_{ib}^{(s)} K_{ii}^{(s)^{-1}} f_i^{(s)})$$

$$= C + \frac{1}{2} \sum_{s=1}^{s=N_s} \Delta u_b^{(s)^T} S_{bb}^{(s)} \Delta u_b^{(s)} \tag{47}$$

where C is a function that does not depend on the parameters $\beta^{(s),j}$. On the other hand, if the effect of interface smoothing is not back-propagated to the substructure interiors (lumped smoothing), $\mathscr{E}(\beta^{(s),j})$ will have a similar expression as (47) but with $K_{bb}^{(s)}$ replacing every occurrence of $S_{bb}^{(s)}$. Minimizing the energy with respect to the smoothing parameters under the conditions (43)

$$\frac{\partial}{\partial \beta^{(s),j}} \left[\mathscr{E} - \tau_j^T \left(\sum_{\Gamma_l^{(s)} \ni j} \beta^{(s),j} - 1 \right) \right] = 0 \tag{48}$$

leads after some algebraic transformations to

$$\boxed{\begin{aligned} &\sum_{\substack{\Gamma_l^{(s)} \ni j \\ s \neq q}} \sum_{\Gamma_l^{(k)} \ni s} \sum_{\substack{\Gamma_l^{(p)} \ni k \\ p \neq s}} \beta^{(p),k} (r^{(q,s),j^T} B^{(s,-),j} [S_{bb}^{(s)}]_{j,k} B^{(s,-),k^T} r^{(p,s),k}) = \tau_j \\ &\qquad\qquad \forall\, j, \quad \Gamma^{(q)} \ni j \\ &\sum_{\Gamma_l^{(s)} \ni j} \beta^{(s),j} = 1 \end{aligned}} \tag{49}$$

where $[S_{bb}^{(s)}]_{j,k}$ is the Schur-complement of $K^{(s)}$ associated with the edges j and k.

Hence, the smoothing parameters $\beta^{(s),j}$ are given by the solution of an auxiliary 'coarse' problem. If the constraints equations (43) are enforced explicitly—that is, the redundant smoothing parameters are eliminated during the setup of the auxiliary problem—the size of this auxiliary problem becomes roughly equal to the number of edges in the substructure problem.

There is no question that the system of equations (49) is awful to read. However, there is also no question that it is easy to program.

4.4. Treatment of a physical crosspoint in the presence of non-conforming interfaces

Assigning a substructure interface node to one and only one substructure edge j (see Eq. (29)), and using the same approximation for all the Lagrange multiplier fields interconnecting any pair of substructures $\Omega^{(s)}$ and $\Omega^{(q)}$ along the edge j, are fundamental to the implementation of the generalized smoothing procedure proposed in this paper. The impact of these two prerequisites on the treatment of a potential physical crosspoint in a substructure problem with non-matching interfaces is as follows (in the case of matching interfaces, our smoothing procedure does not require a special treatment for the crosspoint).

Consider the 'T' three-substructure problem with incompatible interfaces depicted in Fig. 16. The two points A and B are the substructure representatives of the same physical crosspoint. In this particular but revealing example, points A and B have the same coordinates, but point C has different ones. In order to respect the two smoothing prerequisites outlined above, we recommend two approaches.

In a first approach, two points A′ and B′ are inserted in the substructures $\Omega^{(1)}$ and $\Omega^{(2)}$, respectively. Point A′ is positioned as to match the first node at the left of point C in substructure $\Omega^{(3)}$, and point B′ is positioned as to match point C. The interface boundary of $\Omega^{(1)}$ is then decomposed into two edges $\Gamma_I^{(1,2)}$ and $\Gamma_I^{(1,3)}$, $\Gamma_I^{(2)}$ is also decomposed in two edges $\Gamma_I^{(2,1)}$ and $\Gamma_I^{(2,3)}$ and $\Gamma_I^{(3)}$ is partitioned in two edges $\Gamma_I^{(3,1)}$ and $\Gamma_I^{(3,2)}$. The advantage of this approach is that it requires few edges, but on the other hand it does not enforce a strong compatibility of the displacement fields between each of the points A and B and any corresponding point on $\Gamma_I^{(3)}$—that is, at the physical crosspoint. Depending on the smoothness of the solution at the physical crosspoint, and the distances between A′ and B′, this may or may not be a problem.

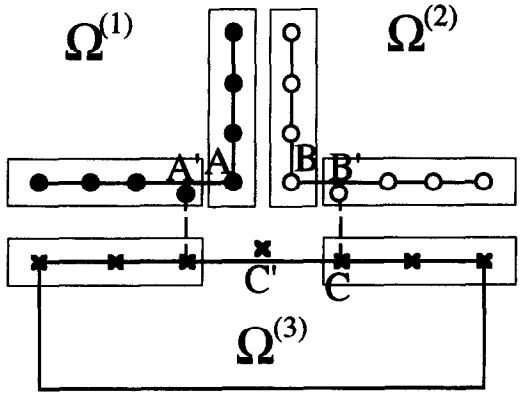

Fig. 16. A 'T' three-substructure problems with a physical crosspoint.

In a second approach, an additional point C′ is inserted at the left of C in $\Omega^{(3)}$ and positioned as to match the points A and B. If required, one more point is also inserted on either $\Gamma_I^{(1,2)}$ or $\Gamma_I^{(2,1)}$ to create two corresponding edges with matching endpoints. This approach generates more edges than the previous one—in particular, each of the points A, B and C′ is now an edge—but enforces compatibility at the physical crosspoint.

5. Applications

Throughout this section, smoothing refers to the 'complete' smoothing procedure determined by Eqs. (12), (24).

5.1. Global/local analysis of a plate problem

First, we demonstrate the two-field hybrid method and smoothing procedure presented in this paper with the global/local analysis of the pressure-loaded plate problem discussed in [8]. In this problem, the maximum stresses are at the midsides of the plate [25]. For obvious symmetry reasons, only a quarter of the structure is discretized and analyzed using 3-node DKT triangular plate elements with 3 d.o.f. per node.

The finite element meshes of the global and local models are depicted in Fig. 17. They contain 143 and 320

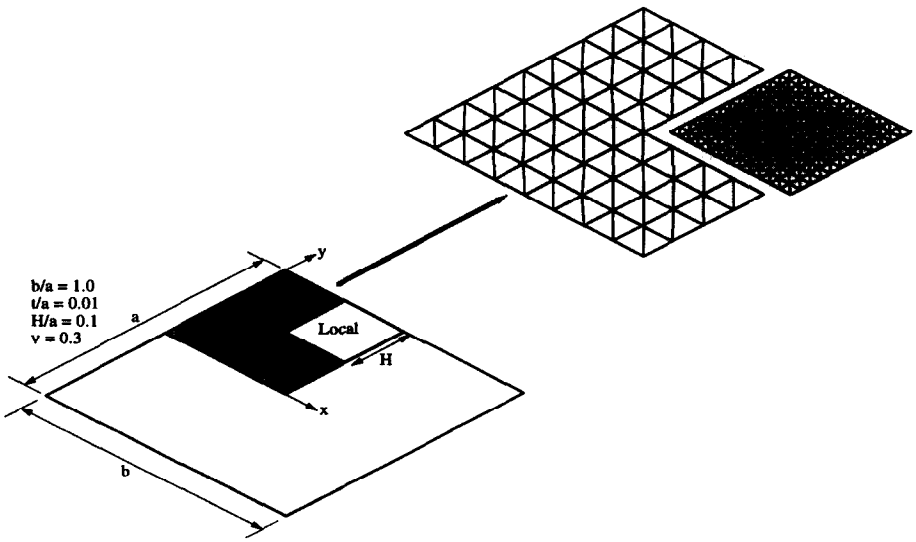

Fig. 17. Global/local analysis of a pressure-loaded plate [8].

Table 1
Global/local analysis of a pressure-loaded plate. Two-field hybrid method with 463 d.o.f. vs. uniformly refined mesh with 7203 d.o.f.

	$\{p_1, p_2\}$	$\{0,0\}$	$\{0,1\}$	$\{1,0\}$	$\{1,1\}$	$\{1,2\}$
$\frac{w_{\max}}{w^{\text{exact}}_{\max}}$	without smoothing	1.012	1.012	1.011	1.011	1.011
	with smoothing ($q=6$)	1.011	1.011	1.011	1.011	1.011
$\frac{\sigma_{\max}}{\sigma^{\text{exact}}_{\max}}$	without smoothing	0.994	0.995	0.998	0.998	0.998
	with smoothing ($q=6$)	0.997	0.998	0.998	0.998	0.998

active d.o.f., respectively, and have non-matching discrete interfaces. The local substructure has been specifically designed to capture the maximum Von Mises stress point. For comparison purposes, a converged finite element solution is computed on a uniformly refined mesh containing 7203 active d.o.f. We refer to the latter solution as the 'exact' solution.

Since in a Kirchhoff plate element the effect of the normal rotation is included in the finite element representation of the transverse displacement, only the continuity of the tangential rotational and vertical displacement d.o.f. are explicitly enforced across the global/local substructure interfaces, using distinct p_1 and p_2 polynomial Lagrange multipliers, respectively. The results of the global/local analysis using the two-field hybrid method with and without a 6th order smoothing are compared in Table 1 with the exact solution (converged finite element solution on the 7203 d.o.f. mesh). In this table, $w^{\max}$ and $\sigma^{\max}$ denote, respectively, the maximum vertical deflection and the maximum Von Mises stress.

Clearly, even for $\{p_1, p_2\}\{0,0\}$—that is, for a constant approximation of the Lagrange multipliers along the interface between the global and local models—the results of the two-field hybrid method are in excellent agreement with the exact solution. Note that in our case, $\{p_1, p_2\} = \{0,0\}$ implies that only 3 Lagrange multipliers are used to connect the global and local model interfaces. In [8], six interface 'pseudo-nodes' and therefore at least 18 Lagrange multipliers are employed with a variant three-field hybrid method to produce a similar accuracy. However, such impressive results are possible only because the displacement solution of the pressure-loaded clamped plate happens to be smooth at the global/local model interfaces. Nevertheless, this also means that the two-field hybrid method is well suited and therefore should be used for this class of applications.

5.2. Analysis of a checkerboard elastomer/steel structure

Next, we consider the plane stress analysis of a two-dimensional structure assembled in a checkerboard fashion from six independently designed cast iron, steel, and rubber squared subcomponents of unit length. The global system is clamped at one end, and subjected to a horizontal and vertical point loads at the top of the other end (Fig. 18). The rubber substructures are characterized by a Young modulus $E^{(1)} = E^{(5)} = E^{(6)} = 5.0 \times 10^7$ N/

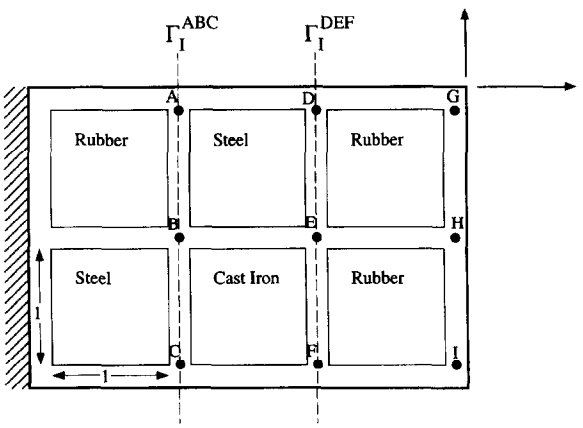

Fig. 18. A checkerboard elastomer/steel structure.

mm^2 and a Poisson ratio $\nu^{(1)} = \nu^{(5)} = \nu^{(6)} = 0.48$, the cast iron subcomponent by $E^{(4)} = 1.025 \times 10^{11}\,N/mm^2$ and $\nu^{(4)} = 0.30$, and the steel substructures by $E^{(2)} = E^{(3)} = 2.05 \times 10^{11}\,N/mm^2$ and $\nu^{(2)} = \nu^{(3)} = 0.3$. Hence, of particular interest in this problem is the high degree of heterogeneity measured by $\alpha = E^{(1)}/E^{(2)} = 2.44 \times 10^{-4}$, and the presence of several crosspoints between extremely stiff and extremely flexible substructures.

We focus on two scenarios where (a) all substructures are discretized into 15×15 4-node plane stress elements with 2 d.o.f. per node and have matching interfaces, and (b) the rubber subcomponents are discretized into 15×15 and the cast iron and steel substructures into 10×10 4-node plane stress elements, and therefore have non-matching interfaces. In scenario (a), the compatibility between the substructure interfaces can be enforced in an exact manner using discrete Lagrange multipliers at every interface d.o.f., in which case the two-field hybrid method produces what we have called throughout this paper the exact solution. However, even in this scenario, we utilize here polynomial Lagrange multipliers in order to illustrate their convergence properties for problems where their use is motivated by the reduction of the computational size of the interface system [14–16], rather than by the non-matching nature of the substructure interfaces. In both scenarios, we apply the two-field hybrid method with and without smoothing. We monitor the quality of the computed

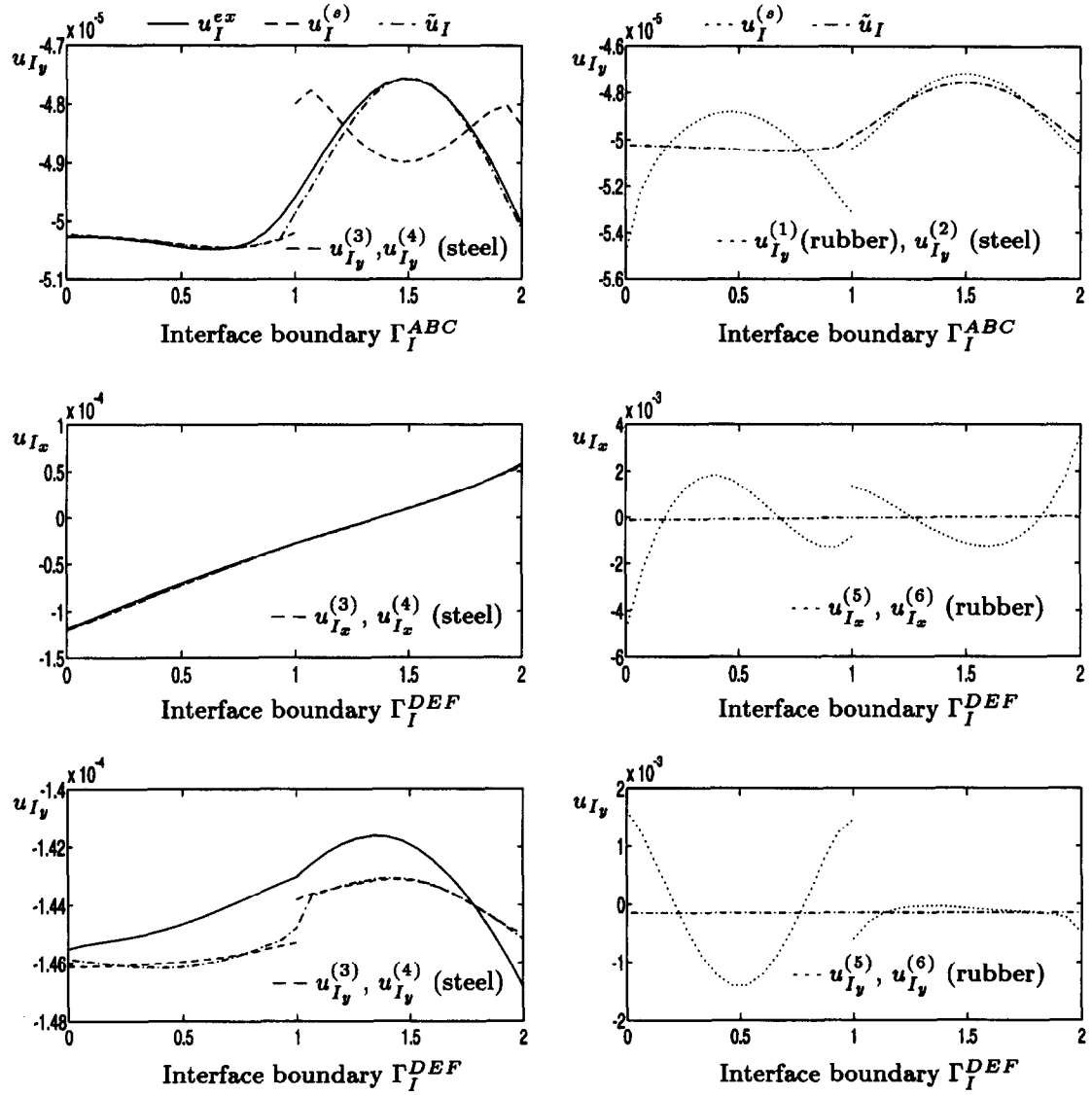

Fig. 19. Predicted horizontal and vertical displacements on Γ_I^{ABC} and Γ_I^{DEF} (matching interfaces—$p = 1$).

solutions at the substructure interfaces $\Gamma_I^{\mathrm{ABC}} = \Gamma_I^{(1,3)} \cup \Gamma_I^{(2,4)}$ and $\Gamma_I^{\mathrm{DEF}} = \Gamma_I^{(3,5)} \cup \Gamma_I^{(4,6)}$, and and the specific points A–I which include two crosspoints.

First, we discuss the solution obtained for scenario (a) where all the sub-components have the same discretization and matching interfaces. We report in Figs. 19–21 the interface displacements computed by the two-field hybrid method, with and without smoothing, for $p = 1, 2, 3$, together with the so-called exact solution. We plot separately the interface displacement fields in the rubber subcomponents and those in the steel and cast iron substructures, because these displacement fields have significantly different magnitudes. The following observations are noteworthy:

- the effects of the strong heterogeneities of this assembly problem are clearly demonstrated by the oscillatory behavior of the non-smoothed solution at the interfaces of the flexible subcomponents and their crosspoints.
- with and without smoothing, the two-field hybrid method is shown to converge when the polynomial degree p is increased.
- however, for an equal p, the two-field hybrid method with smoothing is shown to be significantly more accurate than without smoothing, especially in the rubber subcomponents and at the crosspoint E. Without

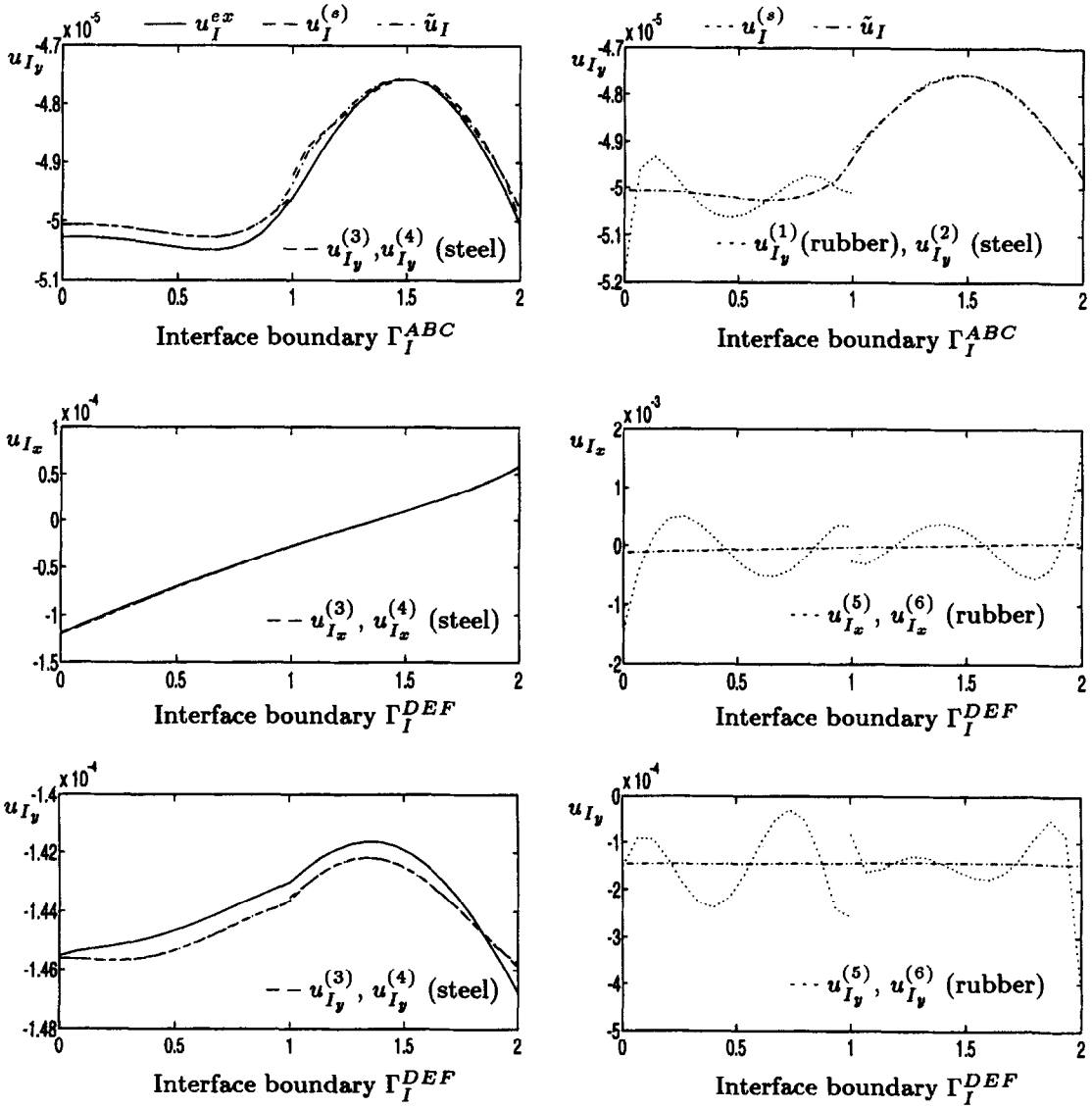

Fig. 20. Predicted horizontal and vertical displacements on Γ_I^{ABC} and Γ_I^{DEF} (matching interfaces—$p = 2$).

smoothing, the trace of the assembled solution on Γ_I^{DEF} is oscillatory. With smoothing, it is in perfect agreement with the exact solution, even for a polynomial degree as low as $p = 1$.

Table 2 reports the relative displacement errors at points A–I for the two-field hybrid method with smoothing. Here again, the effect of the strong heterogeneities appears in the behavior of the solution at crosspoint H. Overall, the treatment of the crosspoints by the proposed smoothing procedure is demonstrated to capture correctly the exact solution.

Next, we focus on scenario (b) where some substructure interfaces do not match because the rubber subcomponents are discretized into 15×15 plane stress elements, while the cast iron and steel subsystems are discretized into 10×10 4-node plane stress elements. We employ the two-field hybrid method with $p = 1, 2, 3$ and apply a 9th order smoothing procedure (see Section 4). We report in Table 3 the relative displacement errors $\epsilon_x^{(s)}$ and $\epsilon_y^{(s)}$ obtained at the control points A, D and G, in the absence and presence of smoothing. Note that in this scenario, the exact solution refers to the two-field hybrid solution computed with $p = 9$ (reference solution). Obviously, this so-called exact solution has two traces on each physical interface connecting two non-conforming substructures, which is why we define in this case $\epsilon_x^{(s)}(i)$ and $\epsilon_y^{(s)}(i)$ at a control point i as follows:

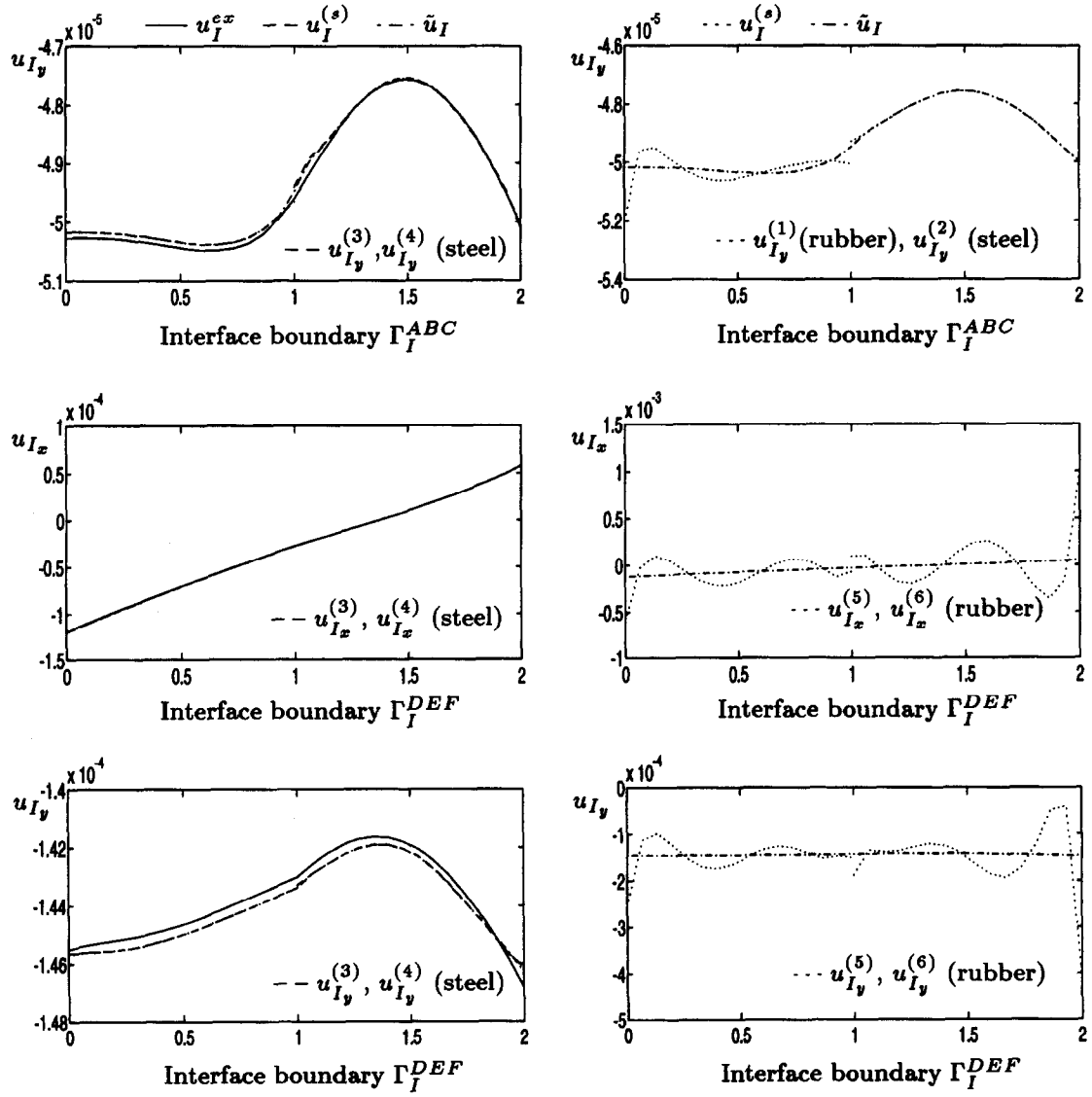

Fig. 21. Predicted horizontal and vertical displacements on Γ_I^{ABC} and Γ_I^{DEF} (matching interfaces—$p = 3$).

Table 2
Coupled analysis of a checkerboard elastomer/steel structure. Conforming substructure interfaces. Two-field hybrid method *with smoothing*. Relative displacement errors at a control point i:

$$\epsilon_x(i) = \frac{|u_x^{ex}(i) - \tilde{u}_x(i)|}{|u_x^{ex}(i)|} \qquad \epsilon_y(i) = \frac{|u_y^{ex}(i) - \tilde{u}_y(i)|}{|u_y^{ex}(i)|}$$

Control point	$p = 1$	$p = 2$	$p = 3$
A	$\epsilon_x = 1.9 \times 10^{-2}$	$\epsilon_x = 1.0 \times 10^{-2}$	$\epsilon_x = 5.9 \times 10^{-3}$
	$\epsilon_y = 9.7 \times 10^{-4}$	$\epsilon_y = 4.2 \times 10^{-3}$	$\epsilon_y = 1.9 \times 10^{-3}$
B	$\epsilon_x = 3.0 \times 10^{-2}$	$\epsilon_x = 7.2 \times 10^{-3}$	$\epsilon_x = 3.5 \times 10^{-3}$
	$\epsilon_y = 5.1 \times 10^{-3}$	$\epsilon_y = 5.0 \times 10^{-3}$	$\epsilon_y = 2.5 \times 10^{-3}$
C	$\epsilon_x = 1.3 \times 10^{-2}$	$\epsilon_x = 1.1 \times 10^{-3}$	$\epsilon_x = 7.4 \times 10^{-5}$
	$\epsilon_y = 1.7 \times 10^{-3}$	$\epsilon_y = 5.2 \times 10^{-3}$	$\epsilon_y = 7.4 \times 10^{-4}$
D	$\epsilon_x = 1.4 \times 10^{-2}$	$\epsilon_x = 8.2 \times 10^{-3}$	$\epsilon_x = 5.0 \times 10^{-3}$
	$\epsilon_y = 2.4 \times 10^{-3}$	$\epsilon_y = 6.8 \times 10^{-4}$	$\epsilon_y = 1.1 \times 10^{-3}$
E	$\epsilon_x = 1.0 \times 10^{-2}$	$\epsilon_x = 1.4 \times 10^{-2}$	$\epsilon_x = 8.3 \times 10^{-3}$
	$\epsilon_y = 1.2 \times 10^{-2}$	$\epsilon_y = 4.3 \times 10^{-3}$	$\epsilon_y = 2.5 \times 10^{-3}$
F	$\epsilon_x = 2.3 \times 10^{-2}$	$\epsilon_x = 8.4 \times 10^{-3}$	$\epsilon_x = 4.7 \times 10^{-3}$
	$\epsilon_y = 1.1 \times 10^{-2}$	$\epsilon_y = 6.1 \times 10^{-3}$	$\epsilon_y = 3.6 \times 10^{-3}$
G	$\epsilon_x = 3.4 \times 10^{-3}$	$\epsilon_x = 9.7 \times 10^{-4}$	$\epsilon_x = 3.9 \times 10^{-4}$
	$\epsilon_y = 8.2 \times 10^{-3}$	$\epsilon_y = 2.3 \times 10^{-3}$	$\epsilon_y = 8.3 \times 10^{-4}$
H	$\epsilon_x = 1.34 \times 10^{0}$	$\epsilon_x = 1.9 \times 10^{-1}$	$\epsilon_x = 1.3 \times 10^{-2}$
	$\epsilon_y = 2.3 \times 10^{-2}$	$\epsilon_y = 9.9 \times 10^{-3}$	$\epsilon_y = 4.4 \times 10^{-3}$
I	$\epsilon_x = 4.7 \times 10^{-2}$	$\epsilon_x = 9.9 \times 10^{-3}$	$\epsilon_x = 3.9 \times 10^{-3}$
	$\epsilon_y = 4.1 \times 10^{-2}$	$\epsilon_y = 9.7 \times 10^{-3}$	$\epsilon_y = 3.6 \times 10^{-3}$

Table 3
Coupled analysis of a checkerboard elastomer/steel structure. Non-conforming substructure interfaces. Two-field hybrid method. Relative displacement errors at three control points

Control point	Smoothing ($q = 9$)	$p = 1$	$p = 2$	$p = 3$
A ($s = 1$)	no	$\epsilon_x = 3.5 \times 10^{-2}$	$\epsilon_x = 1.8 \times 10^{-2}$	$\epsilon_x = 2.9 \times 10^{-3}$
	yes	$\epsilon_x = 5.2 \times 10^{-2}$	$\epsilon_x = 4.4 \times 10^{-2}$	$\epsilon_x = 3.8 \times 10^{-2}$
	no	$\epsilon_y = 1.0 \times 10^{-1}$	$\epsilon_y = 4.3 \times 10^{-2}$	$\epsilon_y = 4.5 \times 10^{-2}$
	yes	$\epsilon_y = 2.2 \times 10^{-2}$	$\epsilon_y = 1.8 \times 10^{-2}$	$\epsilon_y = 2.1 \times 10^{-2}$
D ($s = 5$)	no	$\epsilon_x = 3.9 \times 10^{+1}$	$\epsilon_x = 1.1 \times 10^{+1}$	$\epsilon_x = 3.9 \times 10^{0}$
	yes	$\epsilon_x = 5.7 \times 10^{-1}$	$\epsilon_x = 1.7 \times 10^{-1}$	$\epsilon_x = 8.0 \times 10^{-2}$
	no	$\epsilon_y = 1.2 \times 10^{+1}$	$\epsilon_y = 3.5 \times 10^{-2}$	$\epsilon_y = 7.5 \times 10^{-1}$
	yes	$\epsilon_y = 1.4 \times 10^{-1}$	$\epsilon_y = 8.8 \times 10^{-3}$	$\epsilon_y = 2.2 \times 10^{-2}$
G ($s = 5$)	no	$\epsilon_x = 1.6 \times 10^{-3}$	$\epsilon_x = 1.2 \times 10^{-3}$	$\epsilon_x = 6.3 \times 10^{-4}$
	yes	$\epsilon_x = 3.4 \times 10^{-3}$	$\epsilon_x = 1.0 \times 10^{-3}$	$\epsilon_x = 4.4 \times 10^{-4}$
	no	$\epsilon_y = 1.1 \times 10^{-2}$	$\epsilon_y = 2.4 \times 10^{-3}$	$\epsilon_y = 9.9 \times 10^{-4}$
	yes	$\epsilon_y = 8.3 \times 10^{-3}$	$\epsilon_y = 2.4 \times 10^{-3}$	$\epsilon_y = 9.2 \times 10^{-4}$

$$\epsilon_x^{(s)}(i) = \frac{|u_x^{(s)ex}(i) - \tilde{u}_x^{(s)}(i)|}{|u_x^{(s)ex}(i)|} \qquad \epsilon_y^{(s)}(i) = \frac{|u_y^{(s)ex}(i) - \tilde{u}_y^{(s)}(i)|}{|u_y^{(s)ex}(i)|} \tag{50}$$

where s refers to the index of each substructure connected to the control point being monitored. In the absence of smoothing, $\tilde{u}_x^{(s)}$ and $\tilde{u}_y^{(s)}$ in Eq. (50) are replaced by $u_x^{(s)}$ and $u_y^{(s)}$.

Clearly, the results reported in Table 3 demonstrate the convergence of the two-field hybrid method and highlight the effectiveness of the smoothing procedure for this problem with heterogeneous and non-conforming substructures. For example, at the control point D where the displacement compatibility turns out to be more challenging than at the two other control points, smoothing is shown to reduce the relative error in the horizontal displacement by two orders of magnitude for any polynomial degree $p \leqslant 3$. In particular, note that the two-field hybrid method with $p = 1$ and smoothing generates a better overall solution than with $p = 3$ and without smoothing.

Finally, we note that for this substructure assembly problem, the displacement solutions computed by the two-field hybrid method with smoothing are almost identical for both conforming and non-conforming discretizations, with less than 1% relative difference at the control points.

5.3. Aeroelastic analysis of a wing-box structure

In most realistic aeroelastic computations, the fluid and structure discretizations have non-matching interfaces. For example, in wing flutter problems, the fluid surface grid is typically finer than the mesh of the skin of the structure, at least in the flow direction. One way of handling this situation is to use a staggered procedure for solving the coupled fluid/structure problem [26], and a geometric pairing algorithm [27] for transmitting the flow pressure and structural displacement fields across both sides of the fluid/structure interface. An alternative approach is to design a skin discretization that matches the fluid surface grid, which on one hand simplifies the coupling of the fluid and structure problems, but on the other hand induces non-matching interfaces between some structural components—for example, between the skin and the stiffeners. In the latter case, the two-field hybrid method with smoothing can be employed for solving the structural problem as illustrated in this section.

Since detailed aeroelastic computations are beyond the scope of this paper, we focus here on a demonstration problem. For this purpose, we consider the idealization of a wing-box structure depicted in Fig. 22. The upper and lower surfaces, defined in this example as two separate substructures Ω^{upper} and Ω^{lower}, represent the upper and lower skins of a given wing. They are clamped at one end, free at the other. The two vertical substructures, Ω^{front} and Ω^{back}, represent two of its stiffeners. The upper and lower skins are subjected to an aerodynamic pressure load whose distribution is graphically depicted in Fig. 23. Four concentrated forces representing the gravity forces are also applied beneath the stiffeners at the engine locations (see Fig. 23). All four substructures have the same material properties $E = 4.176 \times 10^9$, $\nu = 0.3$, a thickness $t = 0.00833$, and are discretized using three-noded triangular DKT based shell elements with six degrees of freedom per node. Two assembly configurations are considered. In configuration $C1$, the substructures have non-matching interfaces but intersect only along element edges (Fig. 24). In that case, each of Ω^{upper} and Ω^{lower} contains 256 elements and 864 d.o.f., Ω^{front} contains 40 elements and 180 d.o.f., and Ω^{back} contains 48 elements and 210 d.o.f. In configuration $C2$, the interface edges of the front and back stiffeners *traverse* the elements of the upper and lower skins (Fig. 25).

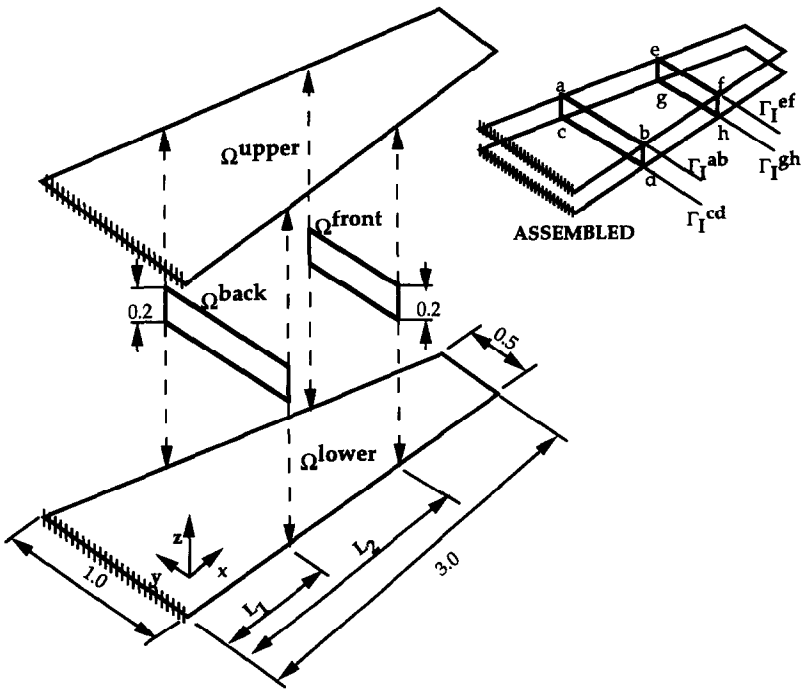

Fig. 22. Idealization of a wing-box structure. Four substructures with non-matching interfaces.

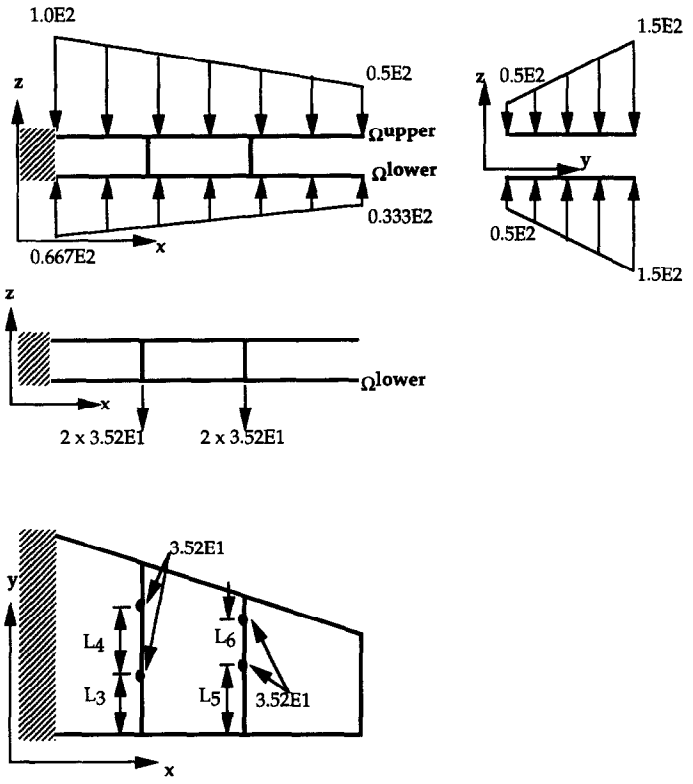

Fig. 23. Load distribution.

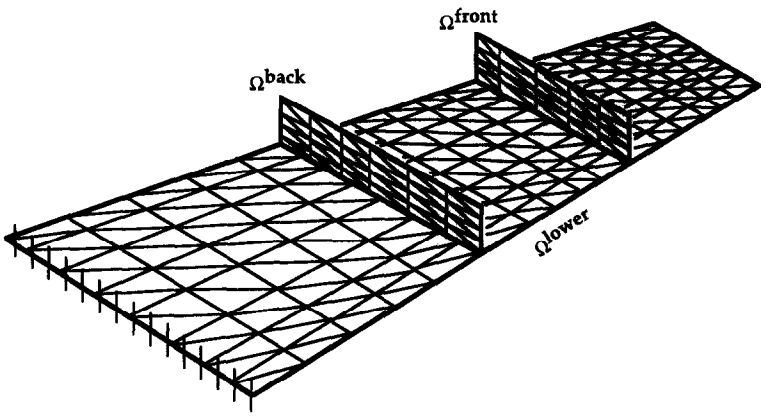

Fig. 24. Non-matching configuration $C1$.

In that case, Ω^{front} contains 64 element and 270 d.o.f., and the other substructures have the same discretization as in configuration $C1$. These two configurations are representative of typical assembly situations. The specific values of the geometric design parameters L_i, $i = 1, \ldots, 6$ (see Figs. 22 and 23) are given in Table 4 for both configurations $C1$ and $C2$. In all cases, the substructure interfaces are denoted by Γ_I^{ab}, Γ_I^{cd}, Γ_I^{ef} and Γ_I^{gh} (see Fig. 22).

In this example, the problem heterogeneities are not induced by different substructure material properties, but by different substructure geometries, orientations, and mesh resolutions. Let u, v, w and θ denote, respectively, the two in-plane displacements, the transverse displacement, and the tangential rotation of the wing-box structure (tangent to a substructure interface) at a substructure boundary interface node. For this example, we use two different approximations of the Lagrange multipliers for gluing the given substructures: (a) polynomial

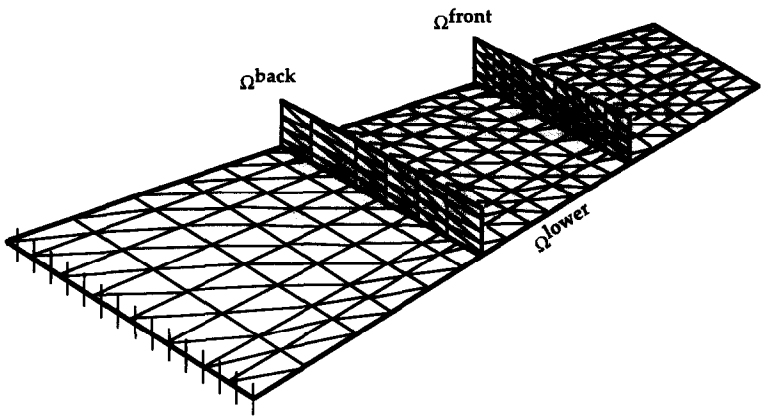

Fig. 25. Non-matching configuration $C2$.

Table 4
Specification of the geometric design variables L_i, $i = 1, \ldots, 6$

Parameter	Configuration $C1$	Configuration $C2$
l_1	0.9375	1.0000
l_2	1.8750	2.0000
l_3	0.4218	0.4166
l_4	0.2813	0.2777
l_5	0.4125	0.3333
l_6	0.2750	0.2500

expressions for the v and θ d.o.f., and (b) cosine expansions for the u and w d.o.f. The cosine approximations are given by

$$\lambda = \sum_{i=1}^{i=n_c} a_i \cos\left(\frac{s}{H_I} \times (i-1) \times \pi\right) \tag{51}$$

where a_i are unknown coefficients, n_c is the number of cosine terms used in the expansion, and s and H_I denote the parametrization and the size of the interface where λ is approximated. The reason for this particular treatment is that on the edges of a DKT element, v and θ are interpolated with linear shape functions, while u and w are interpolated with cubic Hermite polynomials. Therefore, u and w require a higher-order glue that would lead to ill-conditioned interface systems if simple polynomial Lagrange multipliers are used [16], and to better conditioned interface systems when cosine expansions, or Chebyshev polynomials, are employed. In general, the convergence of cosine approximations can be slow. However, cosine approximations of the Lagrange multipliers are well suited for this problem because the u and w displacement fields are discretized with C^1 functions, which implies that they have *continuous derivatives*, and therefore generate continuous stress fields that are approximated here by Lagrange multipliers.

The different values of the polynomial degrees p and number of cosine terms n_c used at the different substructure interfaces are summarized in Table 5 (configuration $C1$) and Table 6 (configuration $C2$) for the target two-field hybrid method as well as for the higher-order reference solution. The smoothing coefficients $\beta^{(s),j}$ associated with the qth order polynomial Lagrange multipliers and/or n_cth cosine expansions are obtained from the solution of the coarse problem (49) and reported in Tables 7 and 8 for the non-matching configurations $C1$ and $C2$, respectively.

A sample of the computed displacement fields are depicted in Figs. 26 and 27. More specifically, Fig. 26 reports the variations of u, v, w and θ on both sides of the interface Γ_I^{gh} for configuration $C1$, and Fig. 27 reports the variations of u, v and w on both sides of the interface Γ_I^{cd} for configuration $C2$. Additionally, the

Table 5
Aeroelastic analysis of an idealized wing-box structure. Polynomial/Cosine approximation of the Lagrange multipliers. Configuration $C1$

Degree of freedom	Polynomial degree p (target solution)	Polynomial degree q reference solution
v on Γ_I^{ab} and Γ_I^{cd}	1	6
v on Γ_I^{ef} and Γ_I^{gh}	1	5
θ on Γ_I^{ab} and Γ_I^{cd}	3	6
θ on Γ_I^{ef} and Γ_I^{gh}	3	5
Degree of freedom	Number of cosine terms n_c (target solution)	Number of cosine terms n_q reference solution
u on Γ_I^{ab} and Γ_I^{cd}	8	14
u on Γ_I^{ef} and Γ_I^{gh}	5	12
w on Γ_I^{ab} and Γ_I^{cd}	8	14
w on Γ_I^{ef} and Γ_I^{gh}	5	12

Table 6
Aeroelastic analysis of an idealized wing-box structure. Polynomial/Cosine approximation of the Lagrange multipliers. Configuration $C2$

Degree of freedom	Polynomial degree p (target solution)	Polynomial degree q reference solution
v on Γ_I^{ab} and Γ_I^{cd}	3	6
v on Γ_I^{ef} and Γ_I^{gh}	3	8
θ on Γ_I^{ab} and Γ_I^{cd}	4	6
θ on Γ_I^{ef} and Γ_I^{gh}	4	8
Degree of freedom	Number of cosine terms n_c (target solution)	Number of cosine terms n_q reference solution
u on Γ_I^{ab} and Γ_I^{cd}	4	14
u on Γ_I^{ef} and Γ_I^{gh}	5	18
w on Γ_I^{ab} and Γ_I^{cd}	3	14
w on Γ_I^{ef} and Γ_I^{gh}	3	18

Table 7
Aeroelastic analysis of an idealized wing-box structure. Smoothing coefficients for the non-matching configuration $C1$

Interface	Substructure	Smoothing coefficient
$\Gamma_I^{gh}\Omega^{\text{lower}}$	Ω^{lower}	0.93
	Ω^{front}	0.07
Γ_I^{ef}	Ω^{upper}	0.62
	Ω^{front}	0.38
Γ_I^{cd}	Ω^{lower}	0.98
	Ω^{back}	0.02
Γ_I^{ab}	Ω^{upper}	0.97
	Ω^{back}	0.03

Table 8
Aeroelastic analysis of an idealized wing-box structure. Smoothing coefficients for the non-matching configuration $C2$

Interface	Substructure	Smoothing coefficient
Γ_I^{gh}	Ω^{lower}	0.43
	Ω^{front}	0.57
Γ_I^{ef}	Ω^{upper}	0.90
	Ω^{front}	0.10
Γ_I^{cd}	Ω^{lower}	0.94
	Ω^{back}	0.06
Γ_I^{ab}	Ω^{upper}	0.96
	Ω^{back}	0.04

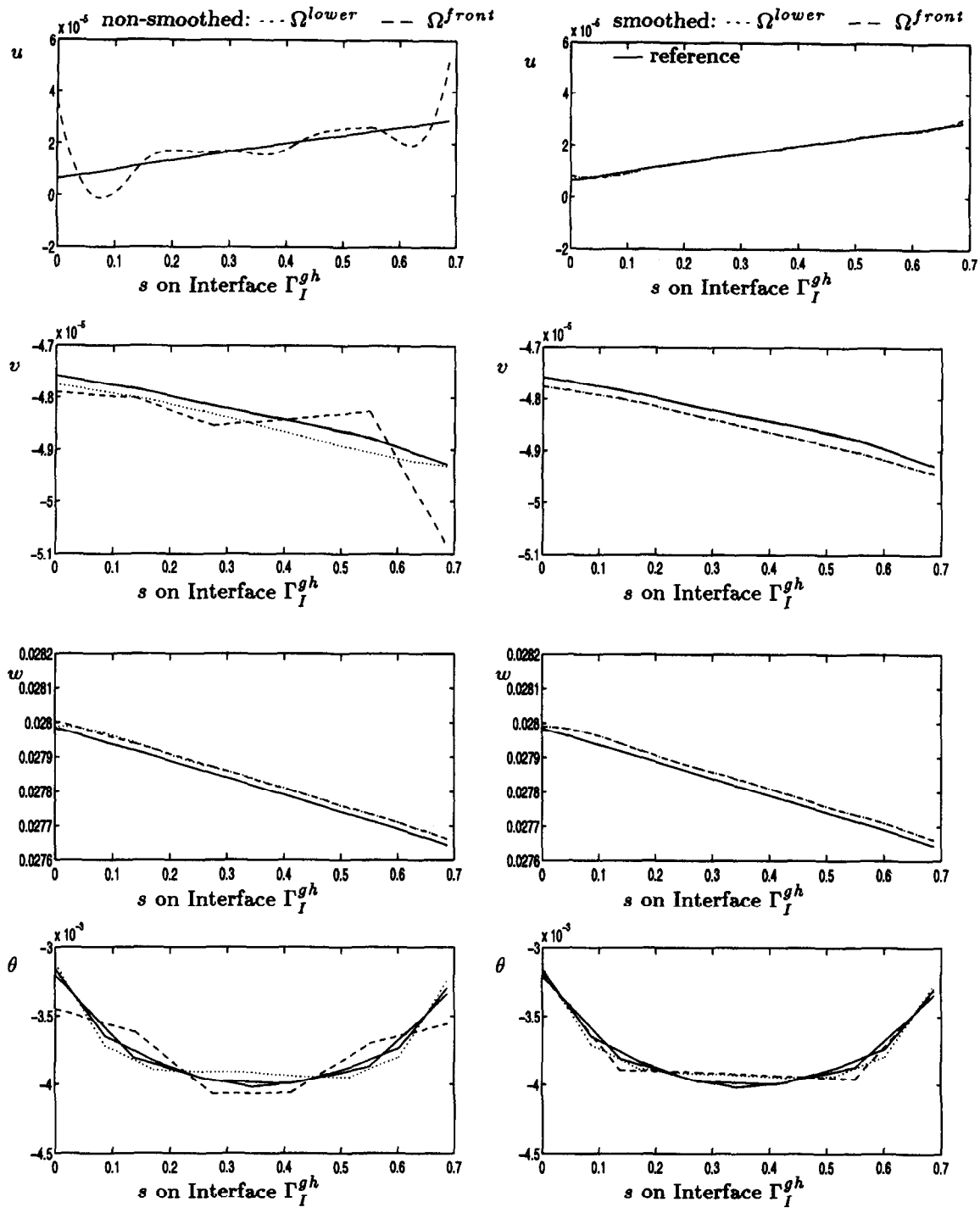

Fig. 26. Predicted displacement fields on Γ_I^{gh} for configuration $C1$.

magnitudes of the substructure relative displacement errors associated with the two-field hybrid method with and without smoothing are summarized in Tables 9 and 10.

Several observations are noteworthy:

- for configuration $C1$, the so-called reference solution is clearly shown to have an almost zero jump across the substructure interfaces. This is not a trivial result given that the substructures of this problem have

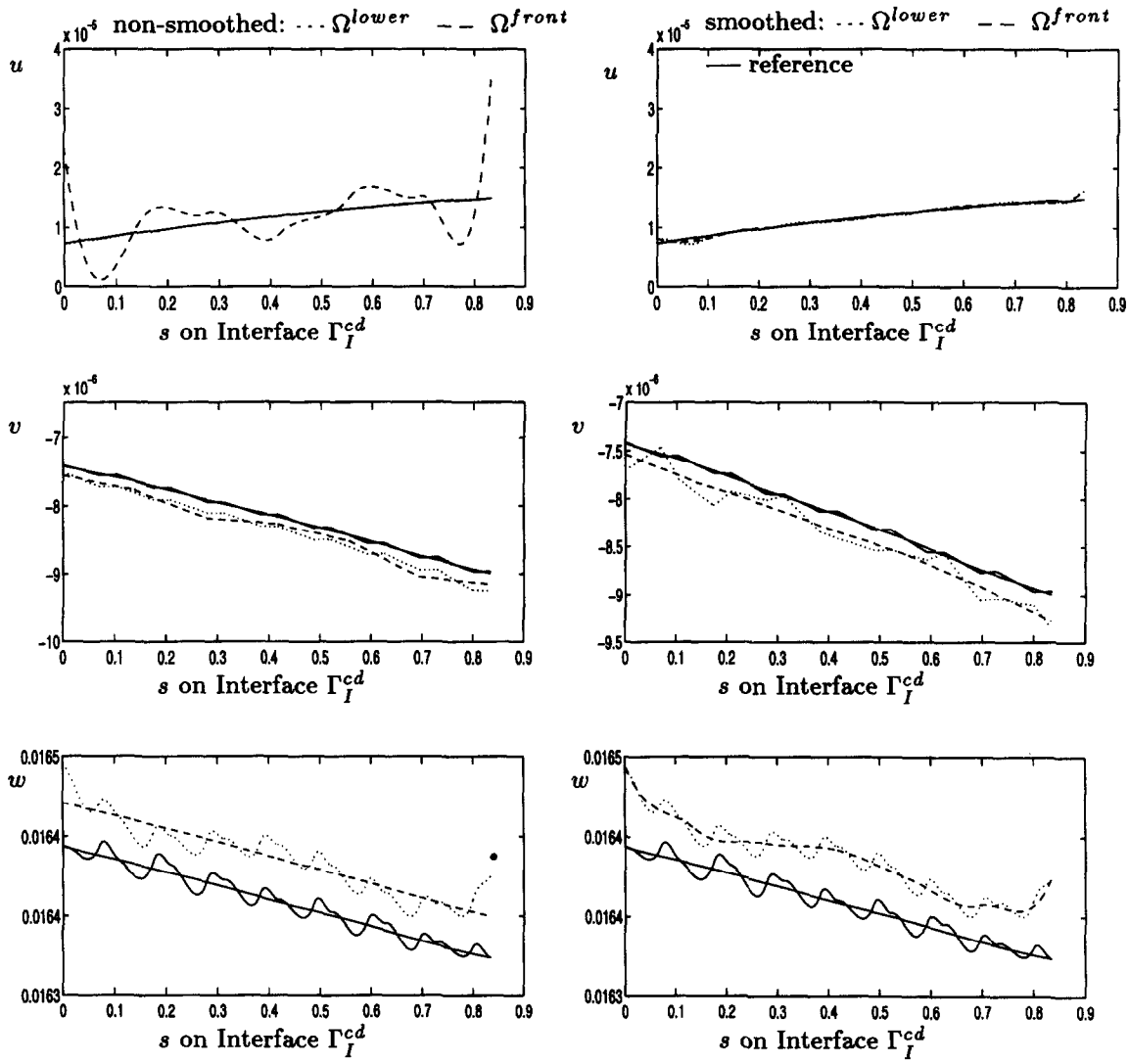

Fig. 27. Predicted displacement fields on Γ_I^{cd} for configuration $C2$.

non-matching interfaces. The same is true for configuration C^2 except for the w field. In that case, the computed reference transverse displacement w exhibits mild oscillations on the interface Γ_I^{cd} of substructure Ω^{lower}. On the other hand, these oscillations are not found in the computed reference w solution on the same interface Γ_I^{cd} but on the side of substructure Ω^{front}. We believe that these mild but spurious oscillations are induced by the fact that the gluing process adopted here assumes a Kirchhoff model inside the DKT element.

- the smoothing procedure is shown to produce two desirable effects: (a) reducing the jump across the substructure interfaces, jump that is noticeable in the non-smoothed case, and (b) generating displacement solutions that are very close to those of the so-called reference solution.
- for this problem, the assembly errors are found essentially in the u field which is a membrane displacement in Ω^{lower} and a transverse displacement in Ω^{front}. Smoothing is shown to eliminate completely these errors. In particular, it is interesting to note that in this case, the smoothing procedure picks up the solution of Ω^{lower}, which is the right thing to do given that Ω^{lower} is stiffer than Ω^{front} in the u direction. Clearly, a simple averaging procedure (50%–50%) would not work in this case.
- quantitatively, the smoothing procedure proposed in this paper is shown to reduce the error in the u displacement field by almost one order of magnitude (see Tables 9 and 10).

Table 9
Coupled analysis of an idealized wing-box structure. Non-matching configuration $C1$. Two-field hybrid method. Magnitude of the substructure relative displacement errors on the interfaces

$$\epsilon_u = \frac{\|u_I^{ex} - \tilde{u}_I\|_2}{\|u_I^{ex}\|_2} \qquad \epsilon_v = \frac{\|v_I^{ex} - \tilde{v}_I\|_2}{\|v_I^{ex}\|_2} \qquad \epsilon_w = \frac{\|w_I^{ex} - \tilde{w}_I\|_2}{\|w_I^{ex}\|_2}$$

Substructure	Without smoothing	With smoothing
Ω^{lower}	$\epsilon_u = 2.8 \times 10^{-3}$	$\epsilon_u = 2.2 \times 10^{-2}$
	$\epsilon_v = 4.1 \times 10^{-3}$	$\epsilon_v = 4.0 \times 10^{-3}$
	$\epsilon_w = 7.2 \times 10^{-4}$	$\epsilon_w = 7.2 \times 10^{-4}$
Ω^{front}	$\epsilon_u = 6.1 \times 10^{-1}$	$\epsilon_u = 9.7 \times 10^{-2}$
	$\epsilon_v = 1.2 \times 10^{-2}$	$\epsilon_v = 4.4 \times 10^{-3}$
	$\epsilon_w = 6.9 \times 10^{-4}$	$\epsilon_w = 6.2 \times 10^{-4}$
Ω^{back}	$\epsilon_u = 8.4 \times 10^{-1}$	$\epsilon_u = 1.8 \times 10^{-2}$
	$\epsilon_v = 3.3 \times 10^{-2}$	$\epsilon_v = 4.3 \times 10^{-3}$
	$\epsilon_w = 7.9 \times 10^{-4}$	$\epsilon_w = 9.0 \times 10^{-4}$
Ω^{upper}	$\epsilon_u = 3.7 \times 10^{-3}$	$\epsilon_u = 4.7 \times 10^{-2}$
	$\epsilon_v = 5.3 \times 10^{-3}$	$\epsilon_v = 4.9 \times 10^{-3}$
	$\epsilon_w = 7.4 \times 10^{-4}$	$\epsilon_w = 7.1 \times 10^{-4}$

Table 10
Coupled analysis of an idealized wing-box structure. Non-matching configuration $C2$. Two-field hybrid method. Magnitude of the substructure relative displacement errors on the interfaces

$$\epsilon_u = \frac{\|u_I^{ex} - \tilde{u}_I\|_2}{\|u_I^{ex}\|_2} \qquad \epsilon_v = \frac{\|v_I^{ex} - \tilde{v}_I\|_2}{\|v_I^{ex}\|_2} \qquad \epsilon_w = \frac{\|w_I^{ex} - \tilde{w}_I\|_2}{\|w_I^{ex}\|_2}$$

Substructure	Without smoothing	With smoothing
Ω^{lower}	$\epsilon_u = 9.4 \times 10^{-3}$	$\epsilon_u = 1.0 \times 10^{-1}$
	$\epsilon_v = 3.0 \times 10^{-2}$	$\epsilon_v = 7.6 \times 10^{-2}$
	$\epsilon_w = 1.3 \times 10^{-3}$	$\epsilon_w = 1.3 \times 10^{-3}$
Ω^{front}	$\epsilon_u = 3.4 \times 10^{-1}$	$\epsilon_u = 5.8 \times 10^{-2}$
	$\epsilon_v = 3.1 \times 10^{-2}$	$\epsilon_v = 3.1 \times 10^{-2}$
	$\epsilon_w = 7.1 \times 10^{-4}$	$\epsilon_w = 8.2 \times 10^{-4}$
Ω^{back}	$\epsilon_u = 1.0 \times 10^{0}$	$\epsilon_u = 5.2 \times 10^{-2}$
	$\epsilon_v = 2.3 \times 10^{-2}$	$\epsilon_v = 2.3 \times 10^{-2}$
	$\epsilon_w = 1.6 \times 10^{-3}$	$\epsilon_w = 2.1 \times 10^{-3}$
Ω^{upper}	$\epsilon_u = 9.5 \times 10^{-3}$	$\epsilon_u = 7.3 \times 10^{-2}$
	$\epsilon_v = 3.0 \times 10^{-2}$	$\epsilon_v = 9.9 \times 10^{-2}$
	$\epsilon_w = 1.4 \times 10^{-3}$	$\epsilon_w = 1.4 \times 10^{-3}$

6. Smoothing vs. higher-order Lagrange multipliers

Solving a substructure assembly problem by a two-field hybrid method with low-order polynomial or piece-wise polynomial Lagrange multipliers and smoothing the computed solution with the Rayleigh–Ritz based procedure proposed in this paper is an alternative to solving the same problem with the same two-field hybrid method but using higher-order Lagrange multipliers. The merits of this alternative are as follows.

- when the two-field hybrid method is used with pth order Lagrange multipliers and the corresponding solution is post-processed with a qth order smoothing procedure where $q \geq p$—for example, $q = 3p$—the size of the interface problem associated with Eqs. (8)

$$\sum_{s=1}^{s=N_s} B^{(s)} K^{(s)^{-1}} B^{(s)^T} \lambda = \sum_{s=1}^{s=N_s} B^{(s)} K^{(s)^{-1}} f^{(s)} \tag{52}$$

is much smaller than in the case where qth order Lagrange multipliers are used—for example, 3 times smaller when $q = 3p$. Of course, this size is also much smaller than that of the interface problem generated

by the mortar method (piece-wise linear Lagrange multipliers on all edges of the interface elements). This computational efficiency is particularly interesting when the two-field hybrid method is used as a mechanism for designing a model reduction algorithm [13–16].

- in general, one does not know a priori the lowest polynomial degree p for which a highly accurate solution is obtained. Opting for an adaptive strategy such as that described in [16] for finding the optimal degree p requires an error criterion and an iterative process. On the other hand, selecting arbitrarily p, for example $p = 3$, and using a qth order smoothing procedure where q is set arbitrarily, for example $q = 9$, produces an excellent solution as demonstrated in Section 5 (see, for example, Table 3), while bypassing the need for an a posteriori error criterion and bypassing iterations.
- when the interface problem (52) is solved iteratively, for example by the FETI method [1,9,11,19], the smoothing procedure presented in this paper can be converted into an efficient preconditioner as shown in [29].

7. Conclusions

The need for assembling independent finite element substructure solutions arises in several engineering and scientific problems including the design and analysis of complex structural systems, component mode synthesis, global/local analysis, adaptive refinement and parallel processing. In this paper, we have discussed the solution of such problems by a two-field hybrid method where the substructures are joined with low-order polynomial or piece-wise polynomial Lagrange multipliers. We have addressed the treatment of crosspoints for non-conforming substructures, exposed the effect of various substructure heterogeneities on the accuracy of the coupled solution, and highlighted the appearance of parasitic eigenmodes and their effect on the prediction of the transient response of a structural system when low-order polynomial Lagrange multipliers are employed. We have also presented a Rayleigh–Ritz based smoothing procedure for addressing all of these issues and improving the accuracy of the computed solution of assembly problems. We have considered both conforming and non-conforming substructure meshes, and demonstrated the benefits of the proposed smoothing procedure with several examples from structural mechanics.

Acknowledgments

We would like to thank Professor Carlos Felippa for his helpful comments on shell problems. The first author acknowledges the support of the Fonds National de la Recherche Scientifique, Belgium. The second author acknowledges partial support by the National Science Foundation under Grant ASC-9217394, and partial support by NASA Langley under Grant NAG-1536427.

References

[1] C. Farhat, A Lagrange multiplier based divide and conquer finite element algorithm, J. Comput. Syst. Engrg. 2 (1991) 149–156.
[2] A.L. Hale and L. Meirovitch, A general substructure synthesis method for the dynamic simulation of complex structures, J. Sound Vib. 69 (1980) 309–326.
[3] C. Farhat and M. Géradin, A hybrid formulation of a component mode synthesis method, AIAA Paper 92-2383, AIAA 33rd Structural Dynamics Meeting, 1992.
[4] C. Farhat and M. Géradin, On a component mode synthesis method and its application to incompatible substructures, Comput. Struct. 51 (1994) 459–473.
[5] C.C. Jara-Almonte and C.E. Night, The specified boundary stiffness/force SBSF method for finite element subregion analysis, Int. J. Numer. Methods Engrg. 26 (1988) 1567–1578.
[6] J.D. Whitcomb, Iterative global/local finite element analysis, Comput. Struct. 40 (1991) 1027–1031.
[7] C. Farhat, L. Crivelli and M. Géradin, On the spectral stability of time integration algorithms for a class of constrained dynamics problems, AIAA Paper 93-1306, AIAA 34th Structural Dynamics Meeting, 1993.
[8] M.A. Aminpour, J.B. Ransom and S.L. McCleary, Coupled analysis of independently modeled finite element subdomains, AIAA Paper 92-2235, AIAA 33rd Structural Dynamics Meeting, 1992.

[9] C. Farhat and F.X. Roux, A method of finite element tearing and interconnecting and its parallel solution algorithm, Int. J. Numer. Methods Engrg. 32 (1991) 1205–1227.
[10] C. Farhat, L. Crivelli and F.X. Roux, A transient FETI methodology for large-scale parallel implicit computations in structural mechanics, Int. J. Numer. Methods Engrg. 37 (1994) 1945–1975.
[11] C. Farhat and F.X. Roux, Implicit parallel processing in structural mechanics, Comput. Mech. Adv. 2 (1994) 1–124.
[12] O.C. Zienkiewicz and R.L. Taylor, The Finite Element Method, 4th edition, Vol. 1 (McGraw-Hill, 1989) 373–396.
[13] M.R. Dorr, On the discretization of interdomain coupling in elliptic boundary-value problems, in: T. Chan, R. Glowinski, J. Periaux and O. Widlund, eds., Second International Symposium on Domain Decomposition Methods for Partial Differential Equations (SIAM, 1989) 17–37.
[14] M.R. Dorr, A domain decomposition preconditioner with reduced rank interdomain coupling, Appl. Numer. Math. 8 (1991) 333–352.
[15] C. Farhat, A saddle-point principle domain decomposition method for the solution of solid mechanics problems, in: D.E. Keyes, T.F. Chan, G.A. Meurant, J.S. Scroggs and R.G. Voigt, eds., Proc. Fifth SIAM Conference on Domain Decomposition Methods for Partial Differential Equations (SIAM, 1991) 271–292.
[16] C. Farhat and M. Géradin, Using a reduced number of Lagrange multipliers for assembling parallel incomplete field finite element approximations, Comput. Methods Appl. Mech. Engrg. 97 (1992) 333–354.
[17] F. Brezzi and M. Fortin, Mixed and Hybrid Finite Element Methods (Springer-Verlag, 1991) 26–27.
[18] Q.V. Dihn, R. Glowinski and J. Periaux, Solving elliptic problems by domain decomposition methods with applications, in: A. Schoenstadt, ed., Elliptic Problem Solvers II (Academic Press, 1984).
[19] C. Farhat and F.X. Roux, An unconventional domain decomposition method for an efficient parallel solution of large-scale finite element systems, SIAM J. Scient. Stat. Comput. 13 (1992) 379–396.
[20] C. Farhat, P.S. Chen and F.X. Roux, The dual schur complement method with well-posed local Neumann problems: regularization with a perturbed Lagrangian formulation, SIAM J. Scient. Stat. Comput. 14 (1993) 752–759.
[21] C. Farhat and M. Lesoinne, Automatic partitioning of unstructured meshes for the parallel solution of problems in computational mechanics, Int. J. Numer. Methods Engrg. 36 (1993) 745–764.
[22] C. Farhat, Fast structural design and analysis via hybrid domain decomposition on massively parallel processors, J. Comput. Syst. Engrg. 4 (1994) 453–472.
[23] I. Babuška, The finite element method with Lagrange multipliers, Numer. Math. 20 (1973) 179–192.
[24] C. Bernardi, Y. Maday and T. Patera, A new non-conforming approach to domain decomposition; the mortar element method, in: Collège de France Seminar, Nonlinear Partial Differential Equations and their Applications, 1990.
[25] S. Timoshenko and S. Woinowsky-Krieger, Theory of Plates and Shells, 2nd edition (McGraw-Hill Book Company, New York, 1959).
[26] S. Piperno, C. Farhat and B. Larrouturou, Partitioned procedures for the transient solution of coupled aeroelastic problems—Part I: model problem, theory, and two-dimensional application, Comput. Methods Appl. Mech. Engrg. 124 (1995) 79–112.
[27] N. Maman and C. Farhat, Matching fluid and structure meshes for aeroelastic computations: a parallel approach, Comput. Struct. 54 (1995) 779–785.
[28] L. Guo-Ping and H. Jiang-Heng, The non-conforming domain decomposition method for elliptic problems with Lagrangian multipliers, Chinese J. Numer. Math. Appl. 15 (1993) 8–19.
[29] C. Farhat and D. Rixen, A new coarsening operator for the optimal preconditioning of the dual and primal domain decomposition methods: application to problems with severe coefficient jumps, Proc. Copper Mountain Conference on Multigrid Methods, Copper Mountain, Colorado, April 3–7, 1995.